TanDEM-X

The 4D Mission Phase for Earth Surface Dynamics: Science activities highlights and new data products after 15 years of bistatic operations

Hajnsek, Irena; Busche, Thomas; Abdullahi, Sahra; Bachmann, Markus; Baumgartner, Stefan V.; Bojarski, Allan; Bueso-Bello, Jose Luis; Esch, Thomas; Fritz, Thomas; Alonso-Gonzalez, Alberto

DOI
10.1109/MGRS.2024.3525403

Publication date
2025

Document Version
Final published version

Published in
IEEE Geoscience and Remote Sensing Magazine

TanDEM-X: The 4D Mission Phase for Earth Surface Dynamics

Science activities highlights and new data products after 15 years of bistatic operations

IRENA HAJNSEK, THOMAS BUSCHE, SAHRA ABDULLAHI, MARKUS BACHMANN, STEFAN V. BAUMGARTNER, ALLAN BOJARSKI, JOSE-LUIS BUESO-BELLO, THOMAS ESCH, THOMAS FRITZ, ALBERTO ALONSO-GONZALEZ, CAROLINA GONZALEZ, LANQING HUANG, THOMAS KRAUS, MARIE LACHAISE, SHIYI LI, FRANCISCO LOPEZ DEKKER, KATHRIN MAIER, MICHELE MARTONE, PIETRO MILILLO, JOSEF MITTERMAYER, MATTEO NANNINI, KONSTANTINOS PAPATHANASSIOU, MATTEO PARDINI, MURIEL PINHEIRO, PAU PRATS-IRAOLA, PAOLA RIZZOLI, MARC RODRIGUEZ-CASSOLA, ACHIM ROTH, MAXIMILIAN SCHANDRI, ROLF SCHEIBER, ULRICH STEINBRECHER, BARBARA SCHWEISSHELM, MICHELANGELO VILLANO, LEENA JULIA WARMEDINGER, BIRGIT WESSEL, GERHARD KRIEGER, MANFRED ZINK, AND ALBERTO MOREIRA

The main goal of the TanDEM-X (TerraSAR-X Add-On for Digital Elevation Measurements) mission is the generation of a global digital elevation model (DEM) of unprecedented accuracy and coverage. The global TanDEM-X DEM product became available in 2016, surpassed all expectations, and became a reference for a wide range of Earth science, commercial, and geospatial applications. In addition, new information products, such as DEM change maps (DCMs), have been developed and are available to the geoscience and remote sensing community. Beyond the operational products, new science applications have been demonstrated and are summarized in this article, along with experimental data acquisitions. This article also aims to provide an overview of science activities with TanDEM-X data and science data acquisitions planned for the coming years.

Digital Object Identifier 10.1109/MGRS.2024.3525403

INTRODUCTION

The German TanDEM-X mission is a bistatic synthetic aperture radar (SAR) mission for scientific and commercial applications [1], [2] and has been in its operational phase, with two radar satellites in close-formation flight, since December 2010 [3], [4], [5], [6]. In this article, we focus on the science activities and review the science applications that have been conducted mainly for 3D and 4D applications. TanDEM-X is delivering data in a single-pass interferometric mode and, with this, providing data in 2D (i.e., range and azimuth), 3D (i.e., adding the height derived from interferometry), and 4D (i.e., 3D data acquisitions over time). TanDEM-X is providing a unique data set to a broad user community and is the only SAR mission to date to deliver 4D data.

The article starts with a short overview of the TanDEM-X mission to explain the imaging capabilities in order to understand the information products that are used to derive

the new applications. Furthermore, a review of the conducted mission phases is provided, being relevant for the data products to establish a time series. Then, the science coordination activities are presented, with valuable statistics on the application distribution. In addition, new operational data products are presented that have been available for several months. The heart of this article is the "Application Domain," section, "Science Domain" where several 3D and 4D applications are presented. We have also included a section on experimental products and applications using different TanDEM-X operation modes that illustrate the innovative character of the mission due to its flexible and reconfigurable imaging capabilities. We close the article with an outlook and lessons learned.

TanDEM-X MISSION OVERVIEW

On 21 June 2010, the *TanDEM-X* satellite was launched and opened a new era in spaceborne radar remote sensing. The first formation-flying radar system [5] was built by extending the TerraSAR-X mission [7] by a second *TerraSAR-X*-like satellite, *TanDEM-X*, as illustrated in Figure 1.

Both satellites carry advanced high-resolution *X*-band (center frequency: 9.65 GHz; chirp bandwidth: up to 300 MHz) SARs, which can be operated in spotlight, stripmap, and scanning SAR (ScanSAR) modes [8]. The so-called helix formation combines a horizontal orbital displacement at the equator (small differences in the right ascension of the ascending nodes) with a vertical separation over the poles (different eccentricity vectors), resulting in a helix-like relative movement of the satellites along the orbit, as sketched in Figure 2. For a complete mapping of Earth with homogeneous height accuracy, the helix formation parameters are regularly adjusted to achieve adequate interferometric baselines [9].

The resulting large single-pass SAR interferometer enables the acquisition of highly accurate cross-track interferograms, not impacted by temporal decorrelation and atmospheric disturbances, as the basis for the global TanDEM-X DEM, which has been defined to meet or exceed the specifications presented in Table 1 [10]. The height values are referenced to the World Geodetic System 84 ellipsoid, and the coverage must reach at least 97% of all land mass. This primary objective of the mission has been achieved, with the global TanDEM-X DEM being well within specification; the achieved absolute height accuracy exceeds the 10-m specification by almost one order of magnitude, and the coverage is close to 99.9% [11], [12].

The scientific exploitation is not limited to the DEM. *TanDEM-X* has unique capabilities, including along-track interferometry (ATI) and new bistatic and multistatic SAR techniques that support numerous secondary mission objectives. Indeed, some of these experiments were directly performed during the DEM acquisition phase, when suitable satellite formation geometries were available. Moreover, regular acquisitions over selected supertest sites enabled multitemporal analyses. A dedicated science phase after the DEM acquisitions included exploitation of up to 4-km horizontal baselines, operation in the so-called dual-receive antenna (DRA) mode, and a period in a pursuit-monostatic flight formation.

In 2017, the decision was made to continue the mission, with a focus on topographic changes. By repeatedly observing certain areas, a time series of data is generated. The data set gradually grows and, in addition to the three spatial dimensions, contains a fourth dimension – time – revealing new previously hidden insights. For example, the growth and degradation of forests can be measured. Repeated

FIGURE 1. The TanDEM-X bistatic single-pass interferometric mission.

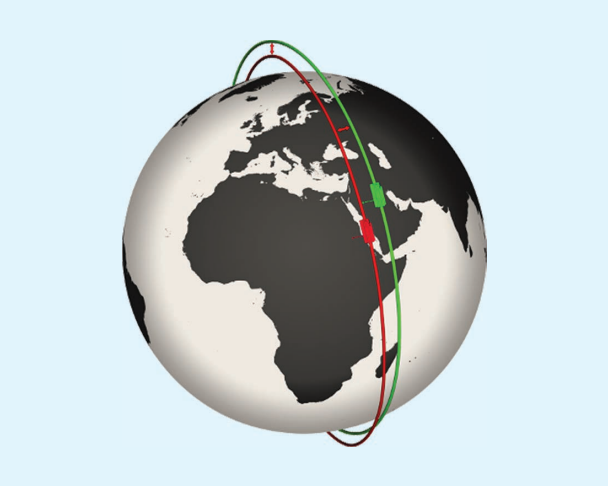

FIGURE 2. The *TerraSAR-X* (red) and *TanDEM-X* (green) satellites flying in a helix formation with horizontal separation at the equator and vertical separation over the poles.

TABLE 1. SPECIFICATIONS OF THE GLOBAL TanDEM-X DEM.

PARAMETER	DEFINITION	REQUIREMENT
Relative vertical accuracy	90% linear point-to-point error in 1 × 1° cell	2 m (slope < 20%) 4 m (slope > 20%)
Absolute vertical accuracy	90% linear error	10 m
Spatial resolution	Independent pixels	12 m (0.4 arcsecond)

height measurements also allow the observation and quantification of the melting of glaciers and ice sheets caused by global warming.

Despite being well beyond their design lifetime, both satellites are still fully functional and have enough consumables for several additional years. Therefore, bistatic operations continue, with a focus on changes in the cryosphere, the biosphere, and densely populated urban areas.

TanDEM-X Mission Phases

In this section, the various DEM and science mission phases since 2010 are presented along with the respective application focus.

Figure 3 shows the different mission phases of TanDEM-X. After the launch of the *TanDEM-X* satellite, a six-month commissioning phase was performed in order to calibrate, verify, and operationalize the mission.

The acquisition of the global DEM started on 11 December 2010. During the next 3.5 years, all land masses were acquired at least twice [13]. The two coverages were planned with different spatial baselines in a ratio of about 0.7. This enabled dual-baseline interferometric processing in order to resolve phase unwrapping errors [14]. On the other hand, the two coverages were combined in order to improve the height accuracy.

Difficult terrains like mountains were acquired several times. They were especially mapped from two different viewing geometries, i.e., in ascending and descending orbit directions, in order to resolve shadow and layover effects [15]. Dry sandy deserts, which suffer from low backscatter, were acquired with steep incidence angles in order to achieve the required height performance [16]. Finally, due to the inclination of the orbit, the inner area of Antarctica, including the South Pole, was mapped in a left-looking mode and using very flat beams for incidence angles up to 60°.

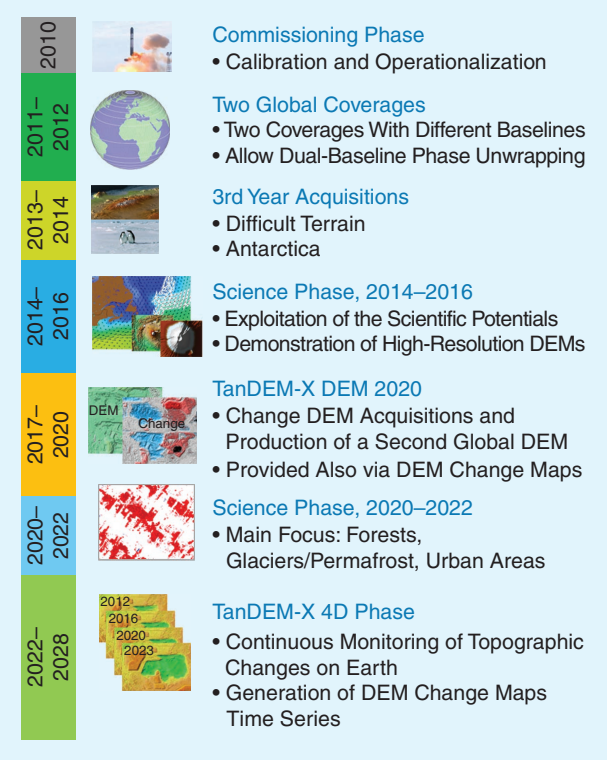

FIGURE 3. The different phases of the TanDEM-X mission.

The global DEM phase was followed by a dedicated science phase. In the first six months of this phase, the satellites were separated in an along-track direction by 10 s (76 km) into a so-called pursuit-monostatic formation. This enabled two independent monostatic acquisitions with the same geometry. During this phase, the formation was not fixed; e.g., the radial baseline experienced its 104-day natural drift. Thus, radial baselines of around 1 km were made possible all over the globe (at a certain time period). The main focus of this phase was measurements in the arctic regions with such large baselines. In addition, the DRA mode was activated, allowing for bistatic quad polarization (quad-pol) acquisitions with four phase centers. The active satellite toggles the transmit polarization between H and V, using the whole antenna. In reception, the antenna is electronically split into two parts, and one part receives H polarization, and the other part receives V polarization. In the pursuit-monostatic formation, this is done on both satellites independently. During the bistatic phases, quad-pol products can be synthesized by toggling the transmit polarization of the active satellite while receiving on one satellite in H and on the other satellite in V polarization [17], [18].

After that, a very large horizontal baseline of about 3.6 km, instead of the 200–500-m horizontal baseline in nominal close formation, was established. This allows accurate monitoring of vegetation growth with decimeter accuracy. The baselines were kept stable for about six months, e.g., during the summer growing season in the northern hemisphere.

Thereafter, an offset in the along-track, i.e., in-flight, direction of a few hundred meters was established in close formation in order to allow for ocean current monitoring. This offset was set such that the along-track separation becomes negligible in northern latitudes (in nominal formations, this is the case only at the poles) in order to avoid temporal decorrelation of the ocean.

Finally, a phase to acquire data for high-resolution DEMs was performed [19]. Dedicated demonstration sites were covered several times with baselines on the order of 1,000 m, enabling products with an independent posting of better than 6 m (compared to 12 m for the global DEM) and with the goal of a relative height error of 0.8 m (compared to 2 m for the global DEM).

In 2017, the TanDEM-X DEM 2020 phase (formerly called the *change DEM phase*) was implemented with the aim to perform an update of the global DEM and to reveal changes in the topography of Earth. This phase lasted for 3.5 years and benefited from the experience gained in the first global DEM phase. Hence, even with a reduced number of acquisitions, complete coverage with good performance

was acquired. The acquisitions from the change DEM phase resulted in publicly available global DCMs and will be processed into the global TanDEM-X DEM 2020 [20], [21].

Starting in 2020, a second science phase was performed. The goal of this phase was the tight monitoring of forests, permafrost areas, and cities.

This phase was continued by the TanDEM-X 4D phase [22]. This phase was planned to last from 2022 until the end of the mission. Here, a biyearly alternation between acquisitions of changing regions with forest and permafrost is foreseen to achieve a temporal timeline of the changing topography of Earth.

Figure 4 demonstrates the interest in the TanDEM-X DEM data by TanDEM-X science users (as of October 2023). The areas with the highest demand are central Europe, the Himalayas, Greenland, the Andes, and the Antarctic Peninsula.

Figure 5 examines the interest in coregistered single-look slant range complex (CoSSC) data. The labels provide the location of exemplary selected supertest sites. The demand for the science supertest sites clearly dominates the picture, with a large number of downloaded scenes per site.

SCIENCE ACTIVITIES COORDINATION

The vast majority of the interferometric SAR (InSAR) data acquired during the mission as well as the DEM products are available to the international science community; exceptions are data acquired for mission maintenance, calibration, and testing, which are available only for the mission ground segment staff. Although some lower-resolution data sets (TanDEM-X 90-m DEM, edited 30-m DEM, DEM 30-m change maps, and polar DEM) and derived data sets (e.g., forest/nonforest mask and global urban footprint) are available through simplified download procedures (partly with registration), in contrary the higher resolution (12-m) global DEM products, and its underlying InSAR (CoSSC) data, are available through a proposal procedure at the German Aerospace Center (DLR) only. The reasons for this are, on the one hand, German legislation (the German Satellite Data Security Act) and DLR export controls within the European Union framework and, on the other hand, the DLR's partnership with Airbus Defense and Space, which holds exclusive commercial exploitation rights for the (high-resolution) DEM and SAR data.

The gateway for international science teams to TanDEM-X science coordination and the interface for TanDEM-X proposal submission at the DLR are offered by the TanDEM-X Science Service System (https://tandemx-science.dlr.de) [1]. Since its launch in 2011, during the commissioning phase, about 6,700 scientists from 130 countries have registered with the TanDEM-X science team. So far during the mission (as of May 2024), 1,936 project proposals, submitted by 1,439 different principal investigators, have been approved by the DLR [1,186 DEM projects, 142 intermediate DEM projects (after one global acquisition), and 608 CoSSC projects]. With an approved proposal and an order account at hand, scientists are able to download global DEM tiles and all kinds of CoSSC data sets through the DLR's EOWEB interface (https://eoweb.dlr.de/egp), which includes all systematic acquired data sets, e.g., for supertest sites, the global DEM (2010–2015), the global DEM 2020 (2016–2020), and all other acquisitions after 2020 and in the coming years. As the high-resolution DEM products in particular are marketed by Airbus Defense and Space within the commercial WorldDEM portfolio, access to these products for scientific applications is quoted, and the amount of data has to be justified in the proposal. Throughout the mission (as of May 2024), about 227,226 products (DEM: 22,355; CoSSC/other SAR products: 204,871) have been delivered to the international science community. The majority of the CoSSC data is connected to application domains, where the detection of changes of glaciers, urban settlements, forests/vegetation, and volcanoes (e.g., glacier mass balance, urban growth, forest height change, and lava volume) are important topics (Figure 6). For DEM proposals (Figure 7), the main topic is geology, with a strong emphasis on tectonics, e.g., to detect and map faults and lineations or to help interpret other structural geology findings. A second large topic is hydrology, where the DEM is used to delineate watersheds, identify a fine flow pattern network, or simulate flooding (Figure 7). The DEM domain "other applications" includes many different topics, with archaeology being one of the main research categories.

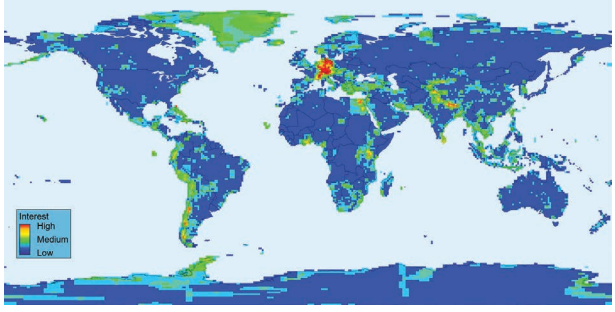

FIGURE 4. A heat map of the interest in the TanDEM-X DEM data by scientific users.

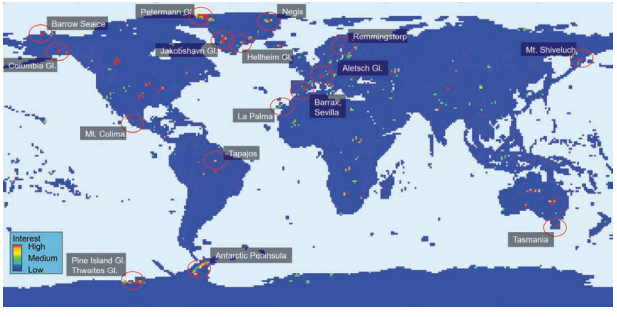

FIGURE 5. A heat map of the interest in the TanDEM-X coregistered single-look slant range complex data by scientific users and the location of selected supertest sites.

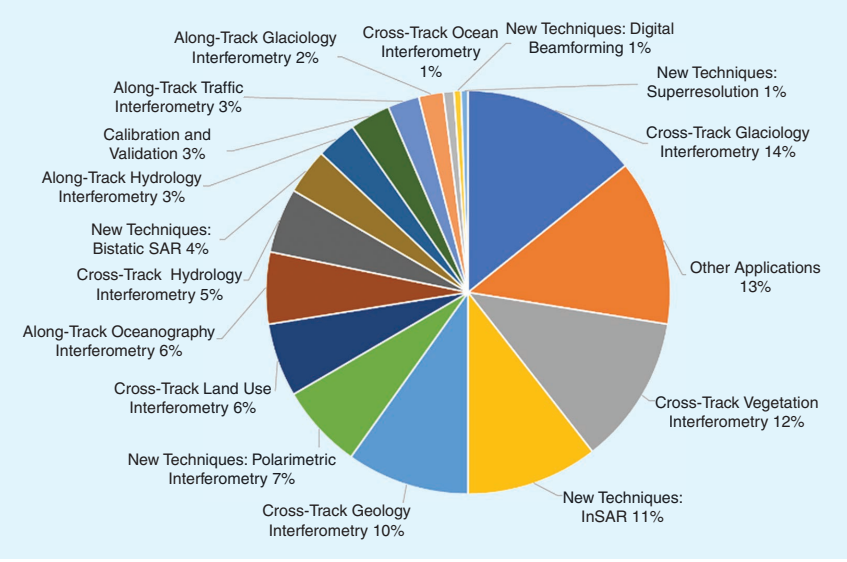

FIGURE 6. The distribution of the CoSSC data requests throughout the application domains.

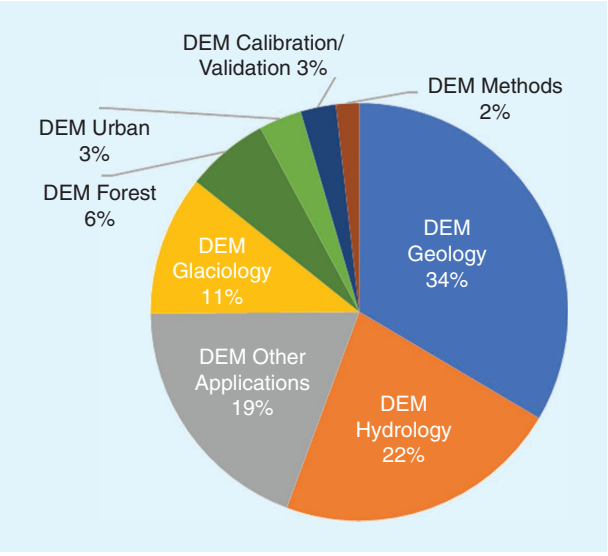

FIGURE 7. The distribution of DEM data requests throughout the application domains.

Since the launch of the mission, science team meetings have been organized at the DLR, in Oberpfaffenhofen, Germany, every second to third year to inform principal investigators about the mission performance and to update the intended mission phases. These meetings are also important to receive feedback from scientists on mission configurations, science phases, and data performance and to trigger exchanges among scientists. The inputs from the meetings are internally evaluated, and some of them are transformed into real actions that are implemented.

In addition to global acquisitions and individual requests for smaller test sites, supertest sites were identified and established. Supertest sites are selected regions for certain domains where TanDEM-X acquisitions have been acquired regularly over the past 13 years and have the size of stripmap acquisitions (15–30 km in width and 50 km in length), and they are listed in "Supertest Sites." The supertest sites were selected at the beginning of the mission as a result of scientific requests and recommendations. In total, 46 test sites were selected, covering agricultural, forest, glacier, sea ice, and volcano test sites worldwide.

TanDEM-X is a highly flexible and reconfigurable mission with many different imaging modes and, in addition to global acquisitions, a large number of future data acquisition requests. This provides a unique opportunity to demonstrate, develop, and test new acquisitions for new and innovative applications, but it also leads to intense support and interaction between the science coordination team and scientists to make a proper selection of the acquisition plan. This circumstance led to a semiautomated science interface and required manual interaction.

The opportunity to combine data acquisition with the Spanish *X*-band satellite *Paz* has led to cooperation between Spain's National Institute of Aerospace Technology and the DLR and provides the benefit of requesting science acquisitions with a shorter repeat time of four, seven, and 11 days. This is especially interesting for highly dynamic applications, which require a shorter repeat time, as with, for example, agricultural crop and snow studies. Performance analysis showed that it is possible to build up high-performance interferograms between the missions [23].

NEW TanDEM-X DIGITAL ELEVATION MODEL PRODUCTS

TerraSAR-X and *TanDEM-X* have been providing high-quality and high-resolution SAR data since 2007 and 2010, respectively, for 17 and 14 years. Since 2016, a global and consistent DEM with unprecedented accuracy has been available, obtained from interferometric data from the TanDEM-X mission [12], [24], [26]. Figure 8 summarizes the various products that were generated with data acquired by the TanDEM-X mission. The DEM and value-added DEM products are presented in this section, while some of the value-added products are discussed in the following sections.

The TanDEM-X 30-m edited DEM (EDEM) and TanDEM-X 30-m DCMs are two products that were released in November 2023. They are globally available for free for science and noncommercial usage in a 30-m posting. The TanDEM-X DEM 2020 was planned to be released by the end of 2024.

PRODUCTS GENERATED FROM ACQUISITIONS BETWEEN 2010 AND 2017

The TanDEM-X DEM was generated from interferometric DEM data acquired over four years, from December 2010 to January 2015. It covers 150 million km^2 of Earth's land mass from pole to pole and has an excellent vertical height error of 1.4-m standard derivation globally. Details of the global TanDEM-X DEM and its quality can be found in [12].

Supertest Sites

TABLE S1. TanDEM-X MISSION SUPERTEST SITES FOR DIFFERENT APPLICATION AREAS.

ID	TEST SITE	COORDINATES (LATITUDE, LONGITUDE)	APPLICATION AREA
1	Barrax, Spain, mixed agriculture	39.067181, −2.158813	Agriculture
2	Demmin agriculture	53.989766, 13.258538	Agriculture
3	Sevilla, Spain, rice agriculture	37.085858, −6.116638	Agriculture
4	Wallerfing agriculture	48.74527, 12.831	Agriculture
5	Injune	−25.295572, 147.65497	Forest
6	Krueger National Park	−24.811668, 31.657104	Forest
7	Krycklan	64.22055, 19.897878	Forest
8	La Selva	10.4209, −84.0224	Forest
9	Remningstorp	58.46202, 13.628747	Forest
10	Tapajos	−3.1148, −54.955	Forest
11	Tasmania northeast forest	−41.679705, 147.854858	Forest
12	Aletsch Glacier	46.502173, 8.033752	Glacier
13	Antarctic Peninsula midwest	−64.599004, −60.859433	Glacier
14	Antarctic Peninsula northeast	−63.984254, −58.773919	Glacier
15	Antarctic Peninsula south	−66.739902, −66.115723	Glacier
16	Antarctic Peninsula southwest	−65.436773, −62.890346	Glacier
17	Antarctic Peninsula mideast	−64.315565, −59.875401	Glacier
18	Bering Glacier	60.432832, −142.797546	Glacier
19	Columbia Glacier	61.378305, −147.062988	Glacier
20	Hellheim Glacier dual-pol	66.3771, −38.2489	Glacier
21	Jakobshavn Glacier	69.117569, −49.570313	Glacier
22	Jakobshavn Inland Glacier	69.14, −49	Glacier
23	Kangerdlugssuaq Glacier	68.668, −32.853	Glacier
24	Petermann Glacier	80.722458, −60.28164	Glacier
25	Pine Island Glacier mid	−75.198609, −99.53626	Glacier
26	Pine Island Glacier north	−75.196072, −98.088726	Glacier
27	Pine Island Glacier south	−75.243818, 100.563795	Glacier
28	Russell Glacier	67.041, −49.834	Glacier
29	Thwaites Glacier north	−75.305306, 106.861204	Glacier
30	Thwaites Glacier south	−75.305306, −106.861204	Glacier
31	Wordie shelf ice	−69.384747, −66.899792	Glacier
32	Alert sea ice ascending orbit 133	82.656652, −62.731934	Sea ice
33	Barrow sea ice	71.467252, −156.952921	Sea ice
34	Asal fault	11.583633, 42.499237	Volcano
35	Bezymianny	55.975924, 160.587021	Volcano
36	Breidamerkurjokull	64.147125, −16.369136	Volcano
37	Colima volcano	19.451053, −103.748971	Volcano
38	El Hierro	27.7431, −18.012772	Volcano
39	Etna	37.740313, 14.983292	Volcano
40	Grimsvotn and Skafta cauldrons	64.433236, −17.510343	Volcano
41	Kilauea east rift zone	19.371721, −155.047302	Volcano
42	Kilauea summit	19.414307, −155.273209	Volcano
43	Merapi volcano	−7.636427, 110.425632	Volcano
44	Piton de la Fournaise	−21.249702, 55.730896	Volcano
45	Shiveluch volcano	56.653333, 161.36	Volcano
46	Soufriere Hills volcano	16.740000, −62.187	Volcano

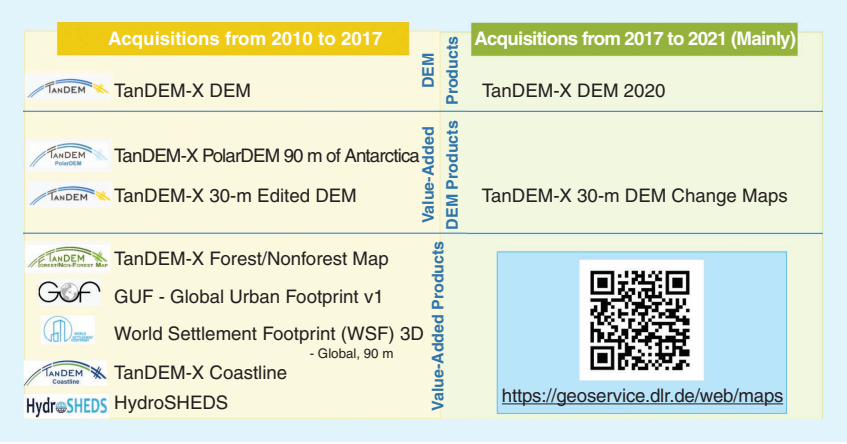

FIGURE 8. The TanDEM-X products for acquisitions from 2010 to 2017 and 2017 to 2021.

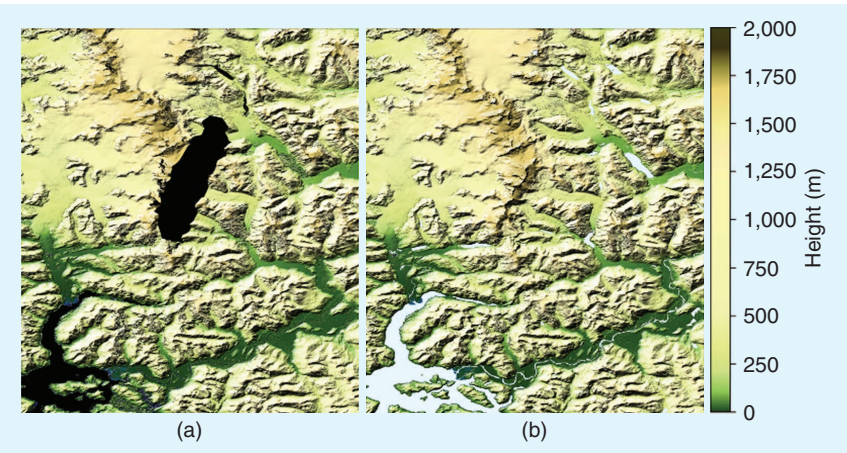

FIGURE 9. A colored hill shade DEM of the Patagonia region: the (a) unedited version (invalid values appear as black pixels) and (b) edited version.

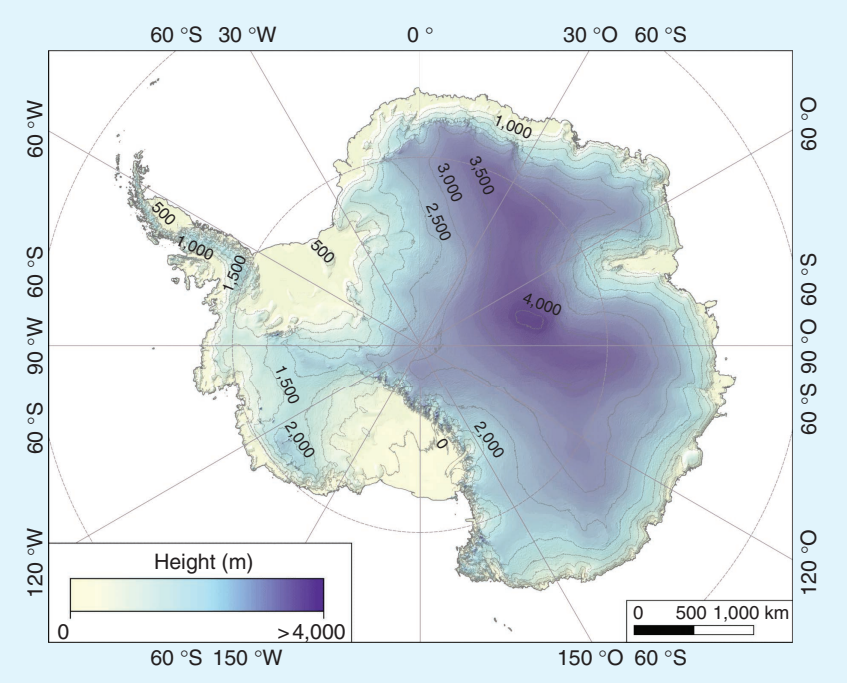

FIGURE 10. The edited 90-m TanDEM-X PolarDEM of Antarctica in color-coded elevations.

The TanDEM-X 30-m EDEM is an edited version of the TanDEM-X global DEM with a pixel spacing of 1 arcsecond (arcsec), corresponding to approximately 30 m at the equator. The editing process was fully automated. First, overlapping pixels between adjacent geocells, which showed some inconsistencies, were properly corrected and homogenized. A consistent water body layer was generated to distinguish between voids and water bodies [27]. Water bodies were classified as oceans, lakes, and rivers. Voids were grouped into gaps and also classified to select the parameters for the filling process. Geocells were merged to process gaps corresponding to more than one geocell. Each gap was then filled using an external reference DEM, and each water body was flattened, mainly using the height of the shoreline as a reference. Finally, an editing mask was generated to identify the editing algorithm used, and, finally, the external reference map was used to fill the gaps. An example of colored hill shade DEMs before and after editing is given in Figure 9. The details of the DEM editing process can be found in [28], and the globally edited version has been published in [29].

Specifically, for polar regions, the TanDEM-X PolarDEM framework provides derivatives of the TanDEM-X DEM [26]. These derivatives include EDEM products, single-year coverages, and penetration bias-corrected DEMs over ice caps worldwide. The edited and reprojected DEM of Antarctica in the universal polar stereographic coordinate system is publicly available at 90 m and is shown in Figure 10 [30].

For ice mass balances, the applicability of a mean DEM over several years is limited. Therefore, especially over Greenland, time-tagged DEMs covering only one winter season are generated (Figure 11). Additionally, these DEMs are corrected regarding the effect of signal penetration to provide a topographic reference for change monitoring in conjunction with optically generated DEMs [31], [32].

To achieve this, a multiple linear regression model is applied to each individual raw DEM before mosaicking. It was shown that the corrections can vary by a few meters per raw DEM, and therefore, this extended procedure significantly improves the estimation of mass changes using TanDEM-X DEMs and reduces under- and overestimation of elevation and mass changes.

PRODUCTS GENERATED FROM ACQUISITIONS BETWEEN 2017 AND 2021

From 2017 until mainly 2021, data for the so-called TanDEM-X 2020 DEM were acquired. The TanDEM-X 2020 DEM is a new and independent DEM covering global landmasses. Hence, it delivers an updated topographic data set and enables monitoring topographic changes on a global scale by comparing the TanDEM-X DEMs from 2010 to 2014 and 2017 to 2021. Thanks to a new phase unwrapping technique originally developed for high-resolution DEMs [33], one coverage will be sufficient for the generation of the TanDEM-X DEM 2020. This goes in line with the reduced possibilities of the overdue mission's satellites. Around 19,780 data takes have been successfully acquired and processed to approximately 200,000 change raw DEMs and CoSSC data [34]. The final mosaicked TanDEM-X DEM 2020 follows technically the same product format specifications as the global TanDEM-X DEM. It has a 12-m posting and similar absolute horizontal and vertical specifications [35]. The absolute height accuracy is comparable to the TanDEM-X global DEM, i.e., on the order of a 1.4-m root-mean-square error (RMSE).

Besides the second global TanDEM-X DEM 2020, a new product, the DCMs, which were released late 2023 in a 30-m (1-arcsec) posting version, have been generated with these acquisitions [36]. The TanDEM-X 30-m DCMs were created to provide global terrain change information that is particularly useful for various fields, including mining, glaciology, and forest monitoring. Hence, they show DEM changes with respect to the first global TanDEM-X DEM in its edited version (TanDEM-X 30-m EDEM) reference for new data collected between 2016 and 2022 (yet, most of the data were taken between 2017 and 2021).

Since these new data are calibrated over stable areas against the TanDEM-X 30-m EDEM, their absolute height accuracy is also in the order of 1 m. The DCMs are annotated with precise time stamps on a pixel basis to enable multitemporal analyses [20]. This product is a first step for visualizing temporal changes in glaciers, ice sheets, coastlines, and forests on a global scale, which is important for understanding the impacts of climate change. Therefore, it is planned to extend the TanDEM-X 30-m DCMs locally to provide detailed information on changes to Earth's surface over time in the form of a stack, or times series, containing all available and future TanDEM-X DEM acquisitions. Figure 12 depicts the height variations in the Kaingaroa Forest, the second-largest forest plantation in the southern hemisphere, on the north island of New Zealand. Acquisitions from mid-2018 and mid-2019 enable not only long-term comparison with respect to the first global DEM (with data collected between 2011 and 2014) but also the monitoring of the plantation within one year. Harvested parcels are shown in darker red, indicating a height change of over 29 m, which is compliant with the height of the planted trees that are Douglas fir (20–100 m high) and radiata pine (15–30 m high).

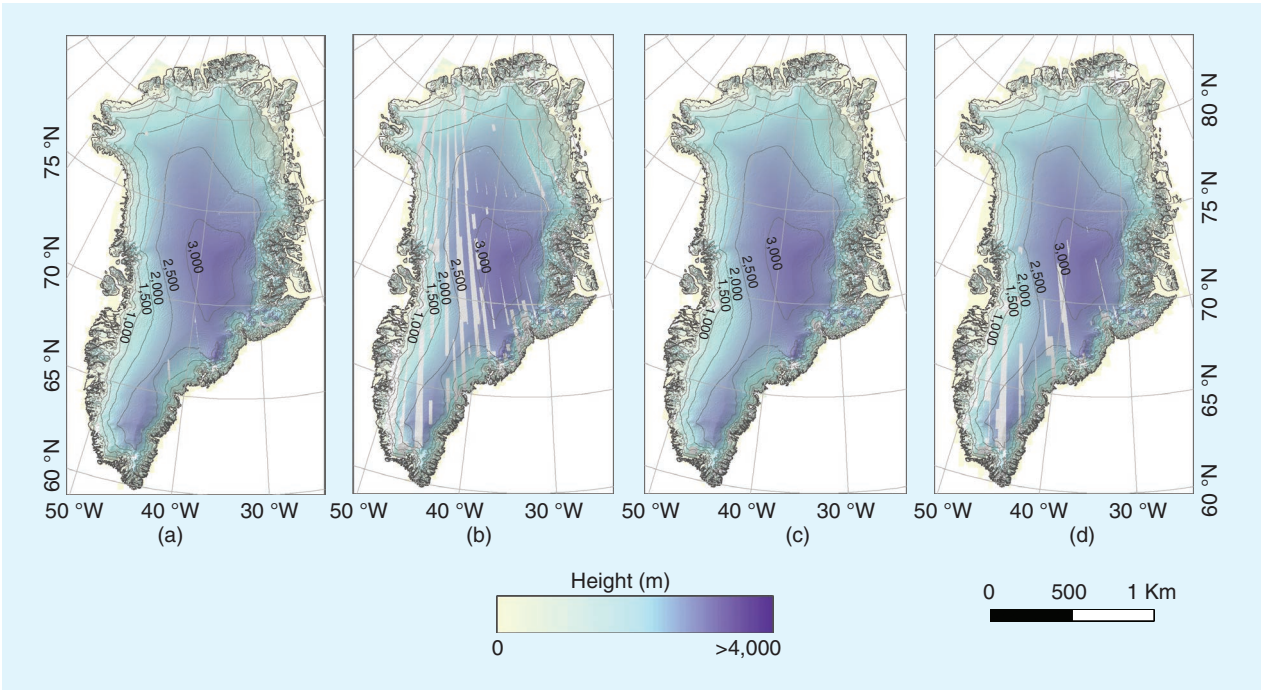

FIGURE 11. Time-tagged DEMs covering winter in (a) 2010–2011, (b) 2011–2012, (c) 2015–2016, and (d) 2016–2017 in color-coded elevations.

This example emphasizes the possibility of using the global DCMs for forest monitoring.

SCIENCE DOMAIN

TanDEM-X has triggered the development of a variety of new applications. In this section, we provide a selection of applications that were developed at the DLR, some with contributions from outside the DLR, that showcase how important the bistatic single-pass interferometric missions are for 3D and 4D applications. The selection is highlighted for different domains, and each section contains a description of the purpose, the methodology, the accuracy, and the needs of the applications.

ANTHROPOSPHERE

URBAN MORPHOLOGY

Characterizing the 3D extent of building stock is crucial for evaluating the efficiency and sustainability of urban development and human activities. The volume and available floor space of buildings significantly impact residents' well-being by influencing their access to housing, productive jobs, and services. Additionally, the 3D density of built spaces affects critical aspects such as the urban climate, emissions, the carbon footprint, transportation, mobility, and the capacity to adapt to natural hazards and climate change. Despite the importance of the building stock for global sustainability and resilience of the built environment, there is limited knowledge about the variations in building area, height, and volume across different countries, cities, and neighborhoods. To address this data and knowledge gap, the DLR developed and processed the global World Settlement Footprint (WSF) 3D data set .

The WSF 3D data set offers measurements of the building fraction, total building area, average building height, and total building volume at a 90-m resolution [37]. It is produced using an enhanced WSF 2019 [38] mask from *Sentinel-1* and *Sentinel-2* satellite imagery, combined with digital elevation data and radar imagery from the TanDEM-X mission. The WSF 3D framework involves three main processing workflows: estimating mean building height from height differences along potential building edges, determining the building fraction and total area within each 90-m cell, and combining this information to calculate average height and total built-up volume. Additionally, global data on skyscrapers and high-rise buildings from the Emporis database are integrated to refine building height and volume measurements. The accuracy of the data set has been validated using high-resolution 3D building models from 19 regions worldwide, covering an area of 85,878 km^2 [37]. The results indicate a mean estimation error of 2.78% for the building fraction, 2.85% (0.22 m) for the building height, and 14.38% for the building volume.

The WSF 3D standard layers (building fraction, total building area, average building height, and total building volume) are accessible for free via the DLR's GeoService of the Earth Observation Center, at https://geoservice.dlr.de/web/maps/eoc:wsf3d. All data sets are provided as Lempel–Ziv–Welch-compressed GeoTIFF files, with each tile covering a 1 × 1° geographical latitude/longitude at a 2.8-arcsec resolution (~90 m at the equator). The latitude resolution decreases in steps toward the poles to account for Earth's reduced circumference.

For the first time, the novel WSF 3D data offer scientists, planners, and policy makers globally consistent wall-to-wall empirical evidence of the key spatial characteristics of the world's building stock. For example, Figure 13 is a 3D representation of average building volumes calculated for concentric rings from the center to the outskirts of the cities of New York (United States), Beijing (China), and Munich (Germany), derived from the WSF 3D data set. This enables a more accurate assessment and deeper understanding of the 3D morphology of the built environment and horizontal and vertical patterns of the megatrend of global urbanization.

BIOSPHERE

FOREST MAPS

The TanDEM-X bistatic interferometric coherence represents a valuable feature for a large variety of applications, being sensitive to the changes in volume scattering. This aspect can be exploited to map forested areas at high resolution

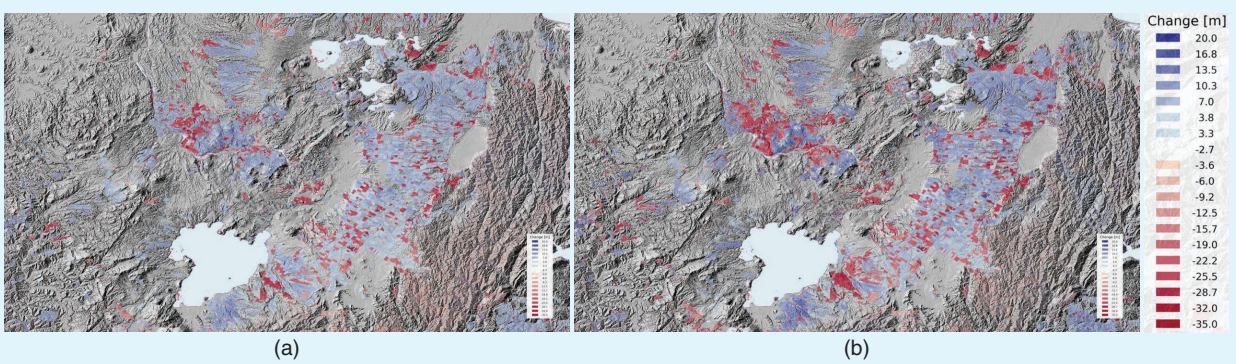

FIGURE 12. TanDEM-X 30-m DCMs over the Kaingaroa Forest on the north island of New Zealand: the (a) DCM from data acquired in mid-2018 overlaid on the EDEM and (b) DCM from data acquired in mid-2019 overlaid on the EDEM.

since radar waves can penetrate into the canopy, leading to volumetric decorrelation [40], [41]. This principle was at the basis of the clustering-based machine learning algorithm developed for the generation of the global TanDEM-X forest/nonforest map [42]. To monitor the temporal evolution of forested areas, a deep learning (DL)-based model was trained, yielding the generation of reliable forest maps for all different bistatic InSAR acquisition geometries. An example is presented in Figure 14, which depicts forested areas as well as deforestation spots in the Amazon rainforests covering the state of Rondonia, Brazil, generated by differentiating the derived forest maps from the TanDEM-X global coverages of 2012–2013 and 2016, respectively [43].

FOREST HEIGHT

Contrary to initial expectations, TanDEM-X has made a significant and unique contribution in a range of forest applications. The sensitivity of the interferometric coherence to the vertical forest structure when, unaffected by temporal decorrelation, combined with the high spatial resolution proved to be valuable for forest applications, compensating in many cases for the limitations imposed by the confined penetration capability into and through vegetation due to the high attenuation rates at the *X* band.

The most prominent example in this context is forest height, where TanDEM-X initiated a large number of studies on forest height estimation from TanDEM-X InSAR data in all possible forest types and conditions [44], [46], [47], [48], [49], [50], [51]. Model-based approaches proved in general to be more robust and with performance that is remarkably good as long as forest conditions allow sufficient penetration to ensure the "visibility" of the whole (vertical) forest extent and as long as the forest (and terrain) heterogeneity can be matched by a simplified parameterization of the vertical reflectivity. While the limited penetration at the *X* band is physical and has to be accepted as long as the underlying topography is unknown [45], the parameterization of the vertical reflectivity profile is constrained only by the number of available measurements in order to obtain a balanced inversion problem.

However, the conventional observation space of TanDEM-X is rather limited. In the global DEM mode, it

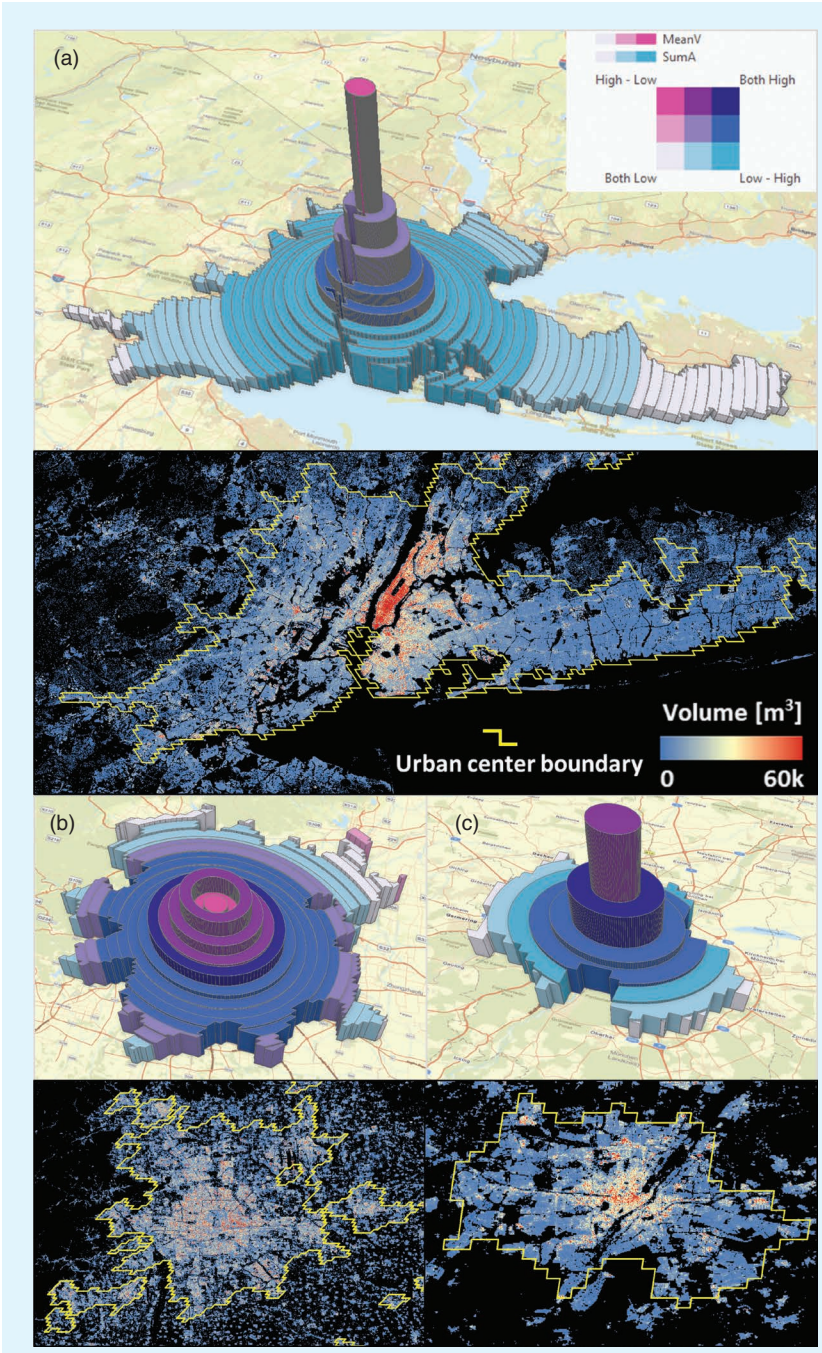

FIGURE 13. The WSF 3D building volume layer for (a) New York City, NY, USA; (b) Beijing, China; and (c) Munich, Germany, with 3D perspective views of the average building volume calculated for concentric rings around the city center. The color coding of the rings displays the bivariate relation between the average volume (MeanV) and the total area of built-up pixels (SumA). The urban boundaries are taken from the Global Human Settlement Layer Urban Center Database of the Joint Research Center of the European Commission.

consists of a single interferogram (at one polarization and a single spatial baseline) per year. The motivation to explore this unique data set triggered approaches based on strong simplifications in the description of the vertical reflectivity and/or relying on the use of external information, such as the use of an external digital terrain model as well as synergetic approaches with other sensors.

In the latter case, the use of lidar measurements to support the model-based inversion of TanDEM-X interferometric data has been investigated in a number of studies [45], [49], [52], [53], [54], [55]. The similarity of the lidar and TanDEM-X measurements, induced by the high sensitivity to the geometrical attributes/architecture of the canopy, high attenuation rates, and high spatial resolution common to both configurations, supports such approaches. The use of lidar waveforms to directly approximate the vertical reflectivity in TanDEM-X interferograms proved to be particularly powerful [55], [56], [57], [58], [59]. This paved the way for combining TanDEM-X and measurements performed by NASA's Global Ecosystem Dynamics Investigation (GEDI) mission, which has operated a waveform lidar on board the International Space Station since the end of 2018. Figure 15 shows a forest height map derived from the combination of TanDEM-X and GEDI measurements with a spatial resolution of 25 m over the Amazon basin. A total of 60 million GEDI measurements and 12,000 TanDEM-X images were combined to produce this map. Such maps are relevant as stand-alone products, recognizing that their relative accuracy is significantly higher than their absolute accuracy, or relevant for filling the spatial gaps in a higher-resolution GEDI product line. Although the accuracy of the results obtained is rather moderate due to the limited observation space, their significance goes well beyond the ability to use TanDEM-X data to produce forest height maps. On the one hand, it demonstrates the potential of single-pass across-track interferometry to characterize consistent 3D forest structure at large scales, even at frequencies where this seemed impossible in the pre-TanDEM-X era, and on the other hand, it allows defining a framework for combining continuous SAR and sparse or even punctual lidar measurements of forest structure [54].

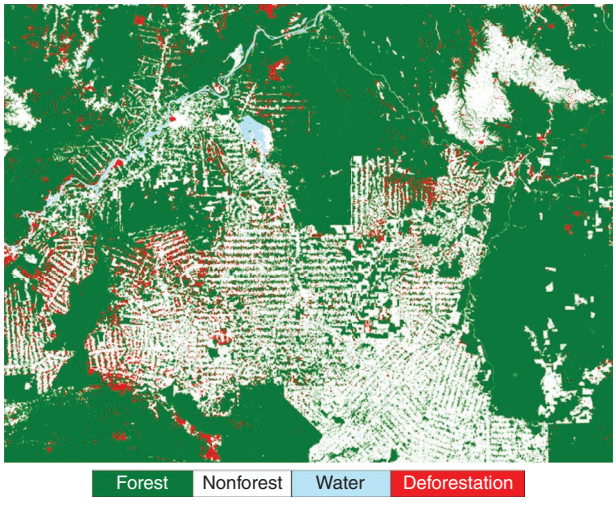

FIGURE 14. Deforestation monitoring in the Amazon rainforest using high-resolution *TanDEM-X* images over the state of Rondonia, Brazil. Forest maps are derived using a DL-based convolutional neural network for semantic segmentation. Deforested areas (in red) are identified by differentiating time-tagged forest maps generated from the *TanDEM-X* global coverage of 2012–2013 and 2016, respectively.

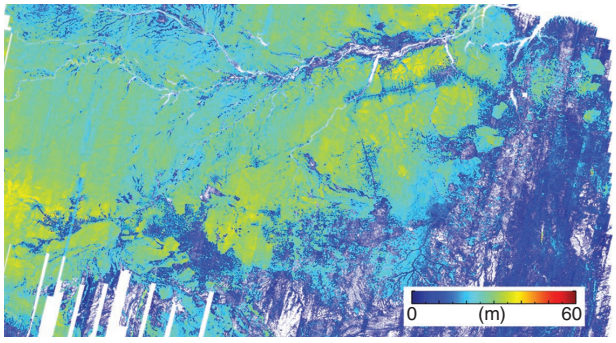

FIGURE 15. A forest height map over the Amazon basin with a spatial resolution of 25 m as derived from the combination of TanDEM-X and GEDI mission measurements. The map extends between 70°W and 45°W in longitude (the horizontal axis) and 15°S and 0° in latitude (the vertical axis).

CROP HEIGHT

The monitoring of agricultural crop development and stages is very important for farmers to identify fast disturbances that may appear within the short growing period and to quantify the productivity of crops. Due to global warming, the growing period and soil water availability are changing. One indicator of change can be the crop height change mapped over fields. The primary objective of the TanDEM-X mission was to generate a high-resolution global DEM of Earth. These baselines, however, are not optimal for agricultural applications, where larger baselines are more appropriate

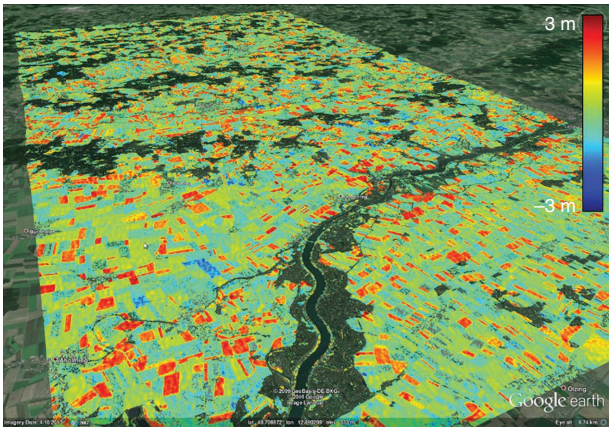

FIGURE 16. A crop height change map between 25 May and 30 July 2015 over the Wallerfing test site in Germany, overlaid on a Google Earth image. The data were acquired during the long-baseline and fully polarimetric phase of the TanDEM-X mission.

for monitoring agricultural vegetation with interferometric techniques. During the experimental phase, in 2015, large baselines with a height of ambiguity of around 5–10 m could be achieved, allowing a sensitivity to crop height changes of 50–100 cm (Figure 16). In addition, fully polarimetric data were acquired in this science phase. The polarimetric and interferometric information was combined to detect changes in different fields and to monitor the crop phenology and evolution over large areas from space. As a main result, plant growth and harvests can be clearly detected, and even height changes of maize crops on the order of 1 m can be properly detected (Figure 17) [60], [61].

CRYOSPHERE

GLACIER DYNAMICS

TanDEM-X elevation models are of great value for monitoring dynamic changes over glaciers and ice caps to reveal specific local dynamics. An example is the multitemporal study performed over the Thwaites Glacier, West Antarctica, where changes in the ice surface elevation were measured with millimeter accuracy, thanks to precise calibration using NASA Operation IceBridge (OIB) measurements [62]. Figure 18 depicts the obtained elevation changes of the ice surface, derived from a time series of TanDEM-X DEMs acquired between 2011 and 2017. This unique capability of TanDEM-X makes it possible to accurately observe changes in surface topography and thus provide in-depth analyses of melt processes in the polar ice caps. In combination with estimations of the grounding line retreat measured using Constellation of Small Satellites for Mediterranean Basin Observation data, the results of the study revealed a complex pattern of retreat and ice melt, with sectors retreating at 0.8 km/year and floating ice melting at 200 m/year, while others retreat at 0.3 km/year, with ice melting 10 times slower. The results were interpreted in terms of buoyancy/slope-driven seawater intrusion along preferential channels at tidal frequencies leading to more efficient melt in newly formed cavities. Such complexities in ice–ocean interaction are not currently represented in coupled ice sheet/ocean models.

GLACIER HEIGHT

Measuring the height changes of glaciers is essential for understanding the dynamics of glacier volume change and mass balance as well as broader implications for climate change, water resources, and sea level change. We employed the geodetic method to measure glacier height changes over time using DEMs collected by the TanDEM-X mission. The TanDEM-X DEMs were generated using the CoSSC product with the InSAR technique. Figure 19 demonstrates the height change of the Great Aletsch Glacier, in the Swiss Alps, and its height loss over the last decade [63], [64]. The figure shows different selected regions, one at a higher altitude (Konkordiaplatz) and one at a lower altitude (the glacier tongue). It is evident that the average height loss is significantly higher at the lower altitude.

GLACIER MASS BALANCE

The glacier-wide mass balance rate is a key variable to characterize the state of health of glaciers, their contribution to river runoff, and sea level rise. The comparison of

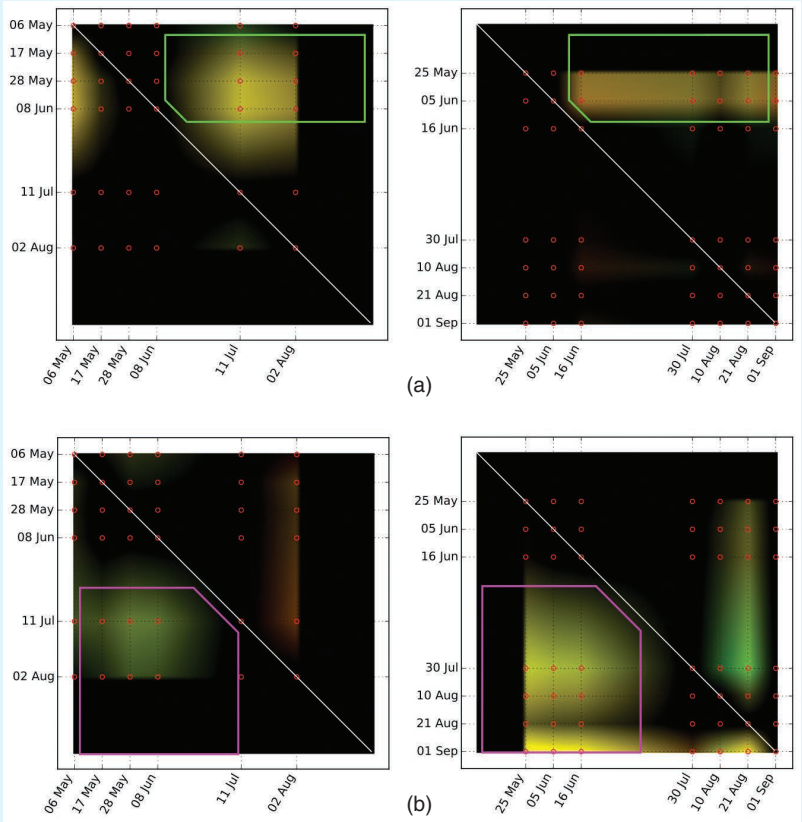

FIGURE 17. A crop growth change analysis with *TanDEM-X* over a maize and rapeseed field, produced during the science phase in 2015. The plots are correlation plots between the different acquisition dates. The red dots in the plots represent the acquisition dates, and the colors within the plots are a combination of the red HH and green VV channels, where yellow represents an equal distribution between red and green. (a) An example of plant growth in the green-marked region, where an increase of intensity is observed. (b) A decrease of intensity during the crop harvest. The two columns are represented by different time series taken between May and September 2015.

multitemporal DEMs, often referred to as the *geodetic method*, has been used for decades to produce maps of glacier elevation changes.

Individual bistatic TanDEM-X acquisitions can be processed to time-stamped DEMs and used to generate time series of surface elevations at yearly or multiyear intervals over regions with high mass losses. After division by the time separation between two surveys, the resulting elevation change rates ($\Delta h/\Delta t$) integrated over the glacier area can be converted into the mass balance using an assumption of the ice density. A comprehensive description of the method is given in [65].

Compared to early volume change assessments, where DEMs from different sensors were combined, the TanDEM-X single-pass interferometer offers a significant improvement in terms of spatial sampling (typically 5–10 m) and vertical accuracy. Typically, elevation changes are measured within ±1-m accuracy if ice-free areas are available for proper adjustment of the DEMs.

Figure 20 conveys the spatial distribution of the elevation change rate of the Southern Patagonian Icefield (SPI) derived from TanDEM-X DEMs acquired in 2012 and 2016 as well as the elevation-dependent $\Delta h/\Delta t$ and area distribution used to calculate the volume change rate. The estimated total SPI mass change for the investigated period was −10.67 ± 1.72 Gt/a [66].

SEA ICE TOPOGRAPHY

The topography of sea ice, encompassing elements like ice ridges, shear zones, rubble fields, and hummocks, is essential for understanding sea ice's interactions with the atmosphere and ocean [67]. While airborne and spaceborne laser altimeters offer precise measurements of sea ice topography, with a vertical accuracy of <1 m, their spatial coverage remains limited. In recent decades, SAR has become a unique remote sensing tool due to its ability to capture imagery regardless of weather and daylight. SAR acquires imagery spanning large swaths, ranging from tens to hundreds of kilometers, while maintaining high spatial resolutions of meters to tens of meters, depending on the mode. However, retrieving sea ice elevation from a single SAR satellite, which requires tens of hours to several days to acquire image pairs, is impractical. The dynamic nature of sea ice results in significant temporal gaps between image acquisitions, leading to substantial interferometric decorrelation and thus impeding the accuracy of height retrieval. Nonetheless, a single-pass SAR interferometer, such as on *TanDEM-X*, offers an unprecedented opportunity to generate a DEM of sea ice despite its dynamic nature [68].

On 29 October 2017, a coordinated campaign between NASA's OIB airborne mission and the DLR's TanDEM-X satellite mission, known as the *OIB/TanDEM-X Coordinated Science Campaign* (*OTASC*), provided a unique opportunity to measure sea ice topography in Antarctica [69]. This campaign was successfully conducted over the western Weddell Sea. Nine dual-pol stripmap TanDEM-X images, overlaid with photogrammetric DEMs from the OIB, were acquired.

In [70], a two-step approach was proposed that integrates sea ice categorization with DEM generation to retrieve sea ice elevation across varying ice classes. In the initial step, sea ice was classified into two categories: small-penetration condition ice and large-penetration condition ice. A random forest classifier, incorporating polarimetric and interferometric features, was employed to identify effective features and categorize the sea ice. In the subsequent step, sea ice DEMs were generated for each type of ice. For small-penetration condition ice, the standard InSAR processing methodology was utilized to retrieve the elevation, given the negligible penetration depth. Conversely, for large-penetration condition ice, the established two-layer-plus-volume model [71] was applied to estimate the InSAR volume decorrelation and shift the InSAR phase center to the top surface, thereby generating an accurate sea ice DEM. The proposed two-step approach was applied over the test site during the OTASC campaign. The SAR-derived DEMs are displayed in Figure 21. The accuracy of the derived DEM

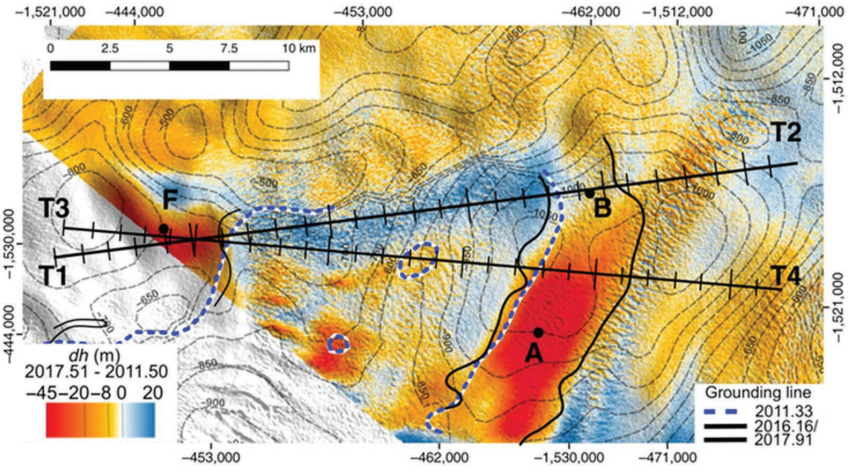

FIGURE 18. Elevation changes (Δh) of the ice surface of the Thwaites Glacier, Antarctica, derived from a time series of TanDEM-X digital elevation models (acquired between 2011 and 2017). Grounding line measurements between 2011 and 2017 derived from Constellation of Small Satellites for Mediterranean Basin Observation data are depicted as well (all corresponding dates are in decimal years). Bold letters T1–T4 identify two transects where additional measurements, i.e., the ice surface elevation from the Airborne Topographic Mapper and ice bottom from the Multichannel Coherent Radar Depth Sounder, were available. Letters *A*, *B*, and *F* refer to specifically analyzed test sites in [62]. The detailed 2D maps of elevation changes from TanDEM-X data can significantly improve the modeling of melting processes and climate change in these sensitive regions.

was validated against coregistered digital surface models, with an RMSE of 0.26 m. This method can also be applied to large regions in Antarctica to retrieve sea ice topography, enabling the study of sea ice dynamics under changing climatic conditions.

IDENTIFICATION OF RETROGRESSIVE THAW SLUMPS

Permafrost is a common feature of Arctic landscapes, and it refers to soil that remains at or below 0 °C for a duration of at least two consecutive years. Permafrost underlies approximately 15% of the landmass in the Northern Hemisphere and is becoming more susceptible to rapid thawing as the climate continues to warm. When ice-rich permafrost thaws, it can alter the surface characteristics of a landscape, which is commonly referred to as *thermokarst*. Retrogressive thaw slumps (RTSs) are emerging as one of the most dynamic types of thermokarst, varying strongly in shape and thawing behavior. High-resolution DEMs are a valuable tool for monitoring surface characteristics of thermokarst features and tracking changes over time, which in turn improves our understanding of large-scale landscape changes and their implications for hydrology, biochemistry, permafrost stability, and hazard risk management. The temporal and spatial sampling and vertical accuracy of the TanDEM-X DEM (10–12-m spatial sampling and approximately 2-m vertical accuracy at a 90% confidence interval) merit investigation for comprehensive monitoring of rapid permafrost thaw and direct retrieval of information on volumetric change rates and, thus, carbon mobilization. This approach has been successfully applied to single-pass InSAR-based time-series DEM analysis to detect and quantify volumetric change rates and potential carbon mobilization of RTSs at several test sites in the Arctic permafrost region [72], [73], [74]. In Figure 22(a), a characteristic RTS is selected, and for each year, the borders are marked in different colors representing the mean height change of the RTS.

GEOSPHERE

LAVA FIELD VOLUME

Multitemporal height differences typically allow for the estimation of changes in the volume of specific target areas on the ground. A paramount application in the geosphere concerns the estimation of lava field volumes after volcanic eruptions. To obtain reliable estimates, an accurate mutual calibration of TanDEM-X time-tagged DEMs prior to differentiation is crucial, given the possible presence of residual offsets and tilts caused by uncertainties in the InSAR geometry retrieval [75]. Figure 23 presents an example of the detected lava field extension and corresponding elevation changes caused by subsequent eruptions of the Fagradalsfjall volcano, Iceland, between 2021 and 2022. The maps were obtained by mutually calibrating and differentiating two TanDEM-X time-tagged DEMs acquired prior to and after the eruptive period, resulting in the estimated volumes of new lava that are reported.

HYDROSPHERE

HydroSHEDS

The HydroSHEDS database provides seamless hydrographic data to support hydroecological research and applications on a regional-to-global scale [76]. The global availability and high accuracy of the TanDEM-X DEM paves the way for

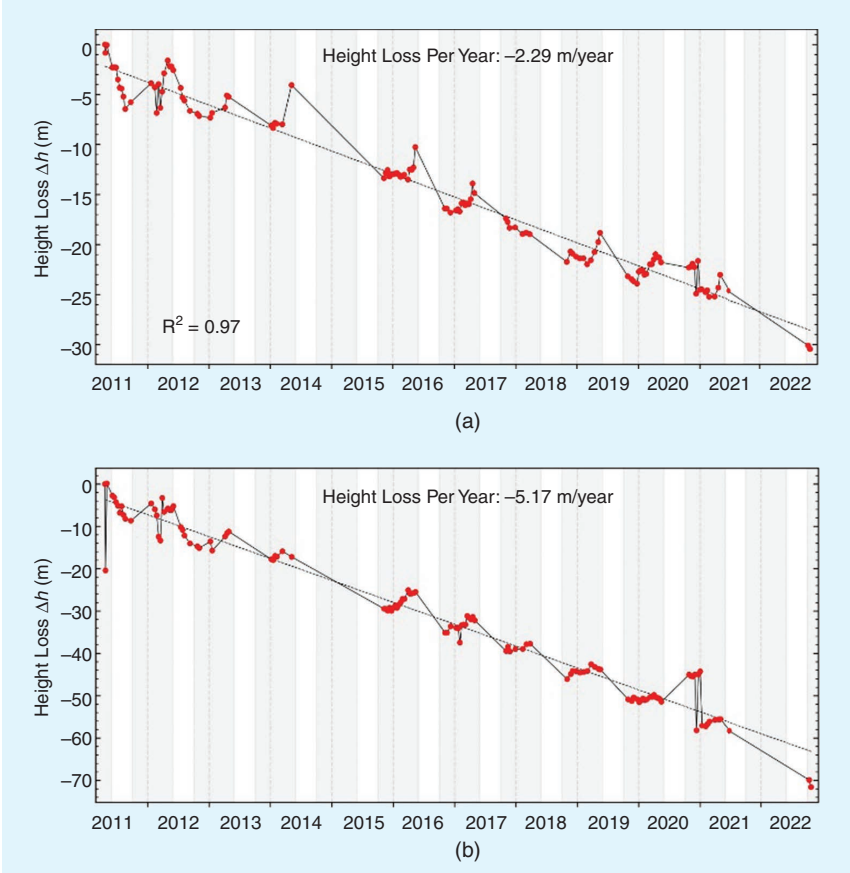

FIGURE 19. The cumulative average height loss over time (2011–2022) [64]: the (a) Konkordiaplatz and (b) tongue area. The cumulative average height loss was calculated relative to the initial measurement on 22 April 2011. Both plots consist of 124 red dots, representing the cumulative height loss at various time stamps between 2011 and 2022. The gray-shaded region highlights the cold season from 1 October to 31 May. The dotted line in each plot indicates the linear regression fit, with the slope coefficient providing the annual height loss rate for the respective area.

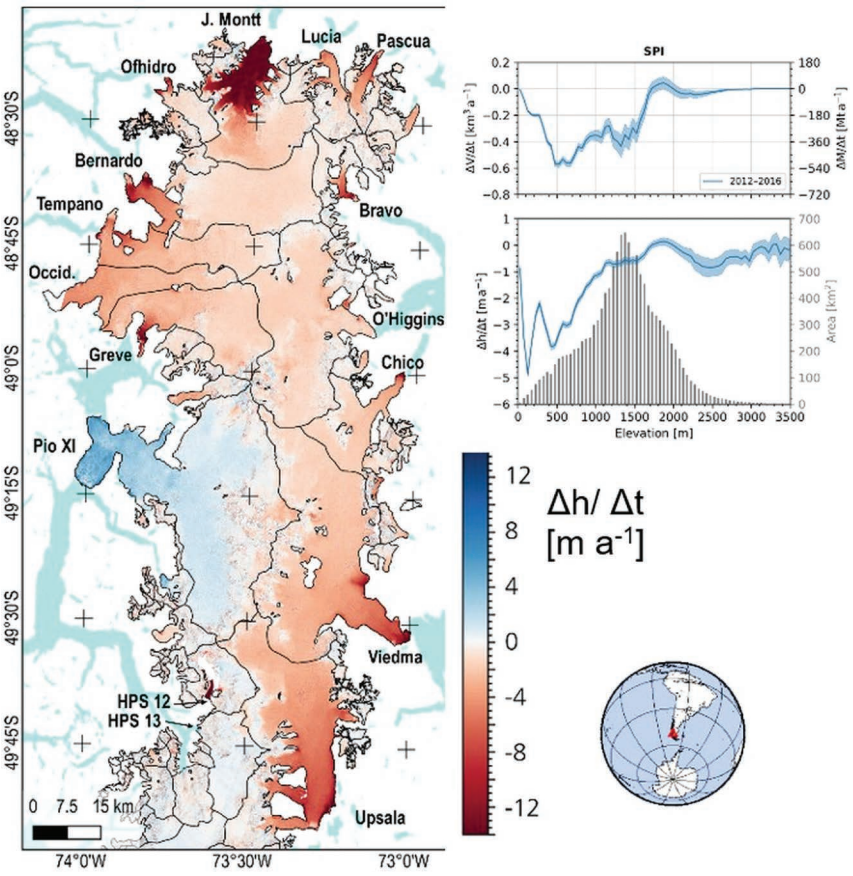

FIGURE 20. The elevation change rate of the Southern Patagonian Icefield (SPI) (12,800 km^2) between 2012 and 2016. Red indicates elevation loss, and blue represents elevation gain. The hypsometric graphs were used to obtain the total mass balance. HPS: Hielo Patagónico Sur.

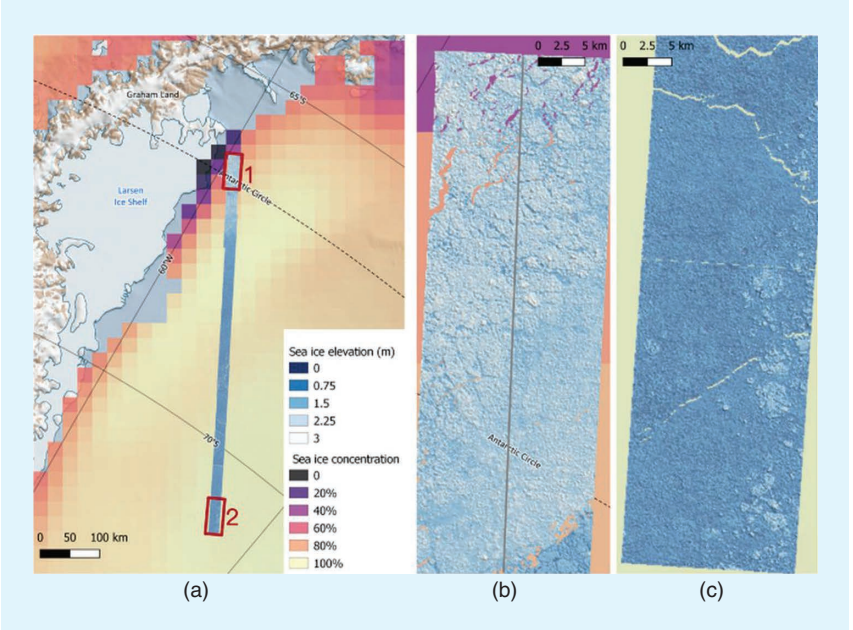

FIGURE 21. (a) The retrieved sea ice elevation from *TanDEM-X* imagery on 29 October 2017, in the Weddell Sea, Antarctica. Zoomed in views of (b) area 1 and (c) area 2. The gray line shows the area overlaid by the digital surface model (reference data).

a second and refined version of the existing and well-established suite of HydroSHEDS products [77]. To derive hydrographic information in the HydroSHEDS format, the underlying DEM, i.e., the TanDEM-X DEM for HydroSHEDS v.2, requires editing. In the preconditioning, voids in the DEM are filled and outliers removed, open-water surface areas are treated by generating and applying a global water mask, and an urban correction is implemented in order to reduce the distortion of streams in built-up areas [78]. The preconditioning is afterward complemented by hydrological conditioning. To obtain drainage pathways, improved stream-burning techniques incorporating recent high-resolution terrestrial open-water masks and advanced methods for tracing centerlines in drainage paths are applied. The resulting core product of HydroSHEDS v.2 is a flow direction raster. From this, other raster products as well as higher-level vector products are derived. The provision of the new HydroSHEDS version will support, e.g., environmental and biodiversity monitoring as well as catchment information for water flow predictions. Figure 24 highlights the improvement of the TanDEM-X-based version 2, as it ensures a more detailed detection of flow paths and streams.

COASTLINE

While the coast in general describes the transition zone between land and ocean, the coastline demarcates the exact boundary between the two spheres. As a feature, the coastline is required in a wide variety of applications covering coastal, littoral, and marine areas. During the editing of the TanDEM-X DEM as a particular application, the coastline defines where ocean heights are to be filled in. For this purpose, a global high-resolution coastline is tailored to and derived from the TanDEM-X DEM in an automatic approach. The method uses the water body mask quality layer of the Copernicus DEM as a

starting point and modifies the original position toward land or ocean based on information from the amplitude and the height error map [26], [79]. To improve the coastline product, the automatic detection is augmented with manual corrections. This targets in particular challenging areas at the transition from inland water to ocean and improves the consistency of the product. This allows fulfilling quality requirements of higher-level applications, such as HydroSHEDS. The coastline of Antarctica has been published as part of the PolarDEM [26], while remaining parts will become available in the shapefile format soon.

EXPERIMENTAL SCIENCE ACHIEVEMENTS

The TanDEM-X formation provides an excellent testbed for future SAR missions and applications. The flexibility in the operation and command of the radar instrument have allowed the execution of several pioneering scientific experiments, some of which represent important milestones in SAR development. A brief description of these achievements is provided in the following sections.

Most of these experiments require dedicated processing beyond the capabilities of the operational processor. For this reason, these data sets

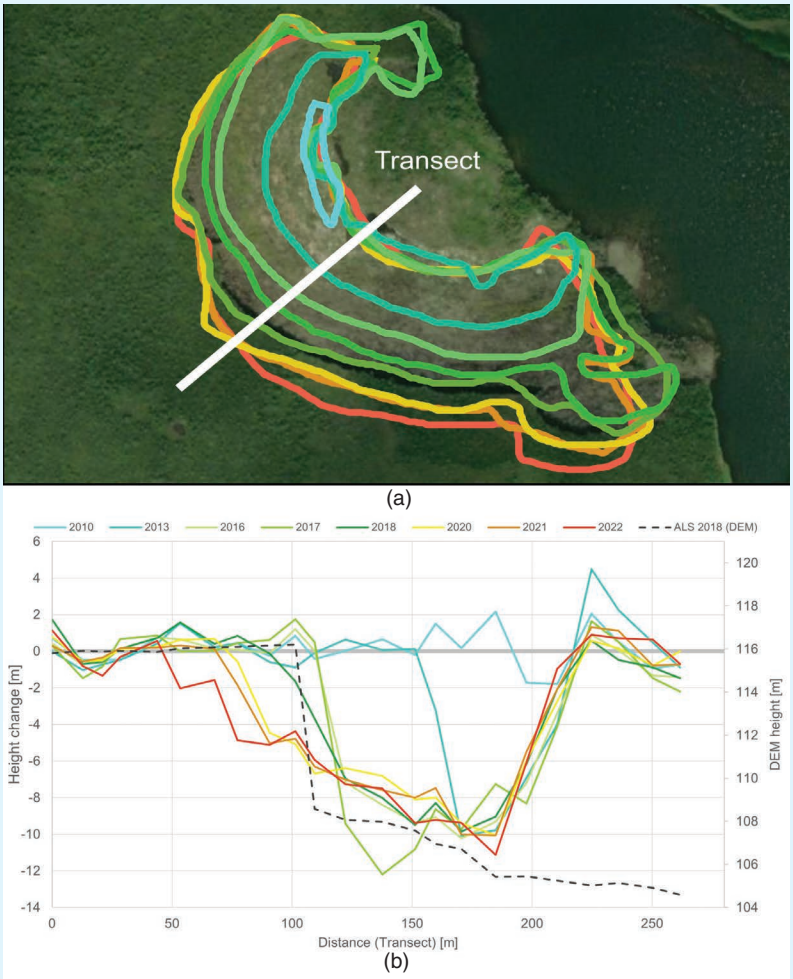

FIGURE 22. A representative RTS with its height changes from 2010 to 2022. (a) The progressive height change over the RTS. (b) A profile of the height change over the marked white line.

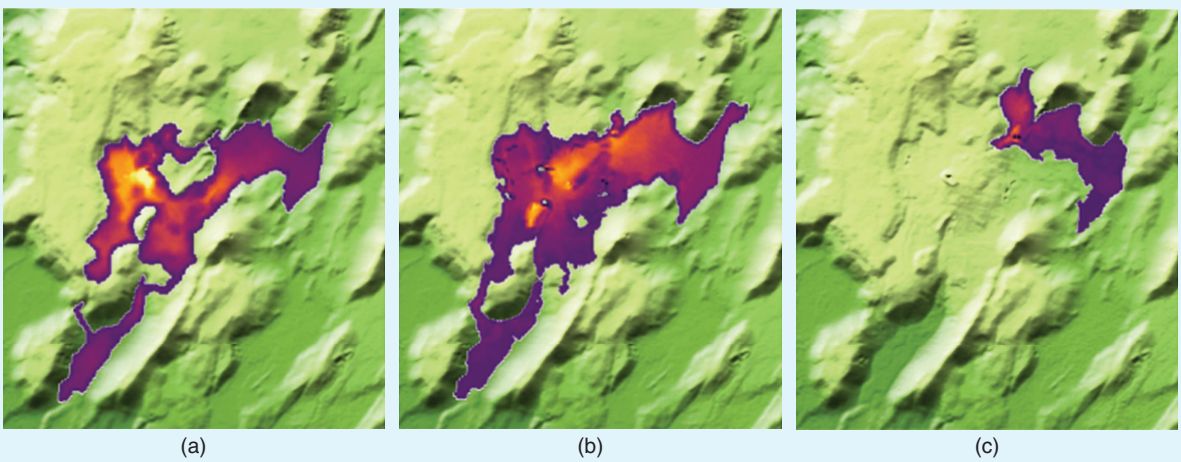

FIGURE 23. Thickness maps derived from the elevation difference corresponding to the lava fields created by subsequent eruptions of the Fagradalsfjall volcano, Iceland, between 2021 and 2022, estimated by differentiating two mutually calibrated TanDEM-X time-tagged DEMs. The TanDEM-X DEM pairs (after–before) were acquired on (a) 18 June 2021–30 October 2020 (corresponding lava volume: ~68.6 million m^3), (b) 19 November 2021–18 June 2021 (corresponding lava volume: ~77.3 million m^3), and (c) 20 December 2022–19 November 2021 (corresponding lava volume: ~11.3 million m^3).

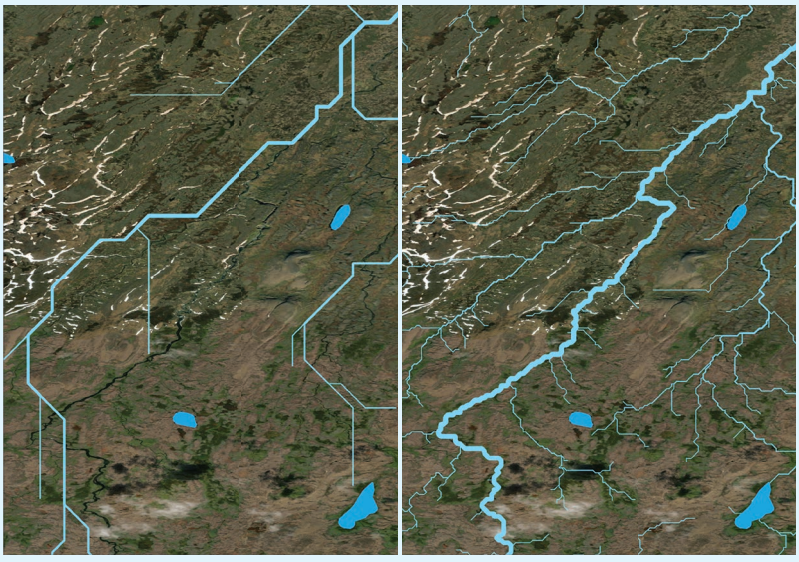

FIGURE 24. A comparison of the stream network of Iceland within the same subset between (a) HydroSHEDS v.1 based on the Shuttle Radar Topography Mission DEM and coarser HYDRO1k elevation data and (b) the refined HydroSHEDS v.2 derived from the TanDEM-X DEM.

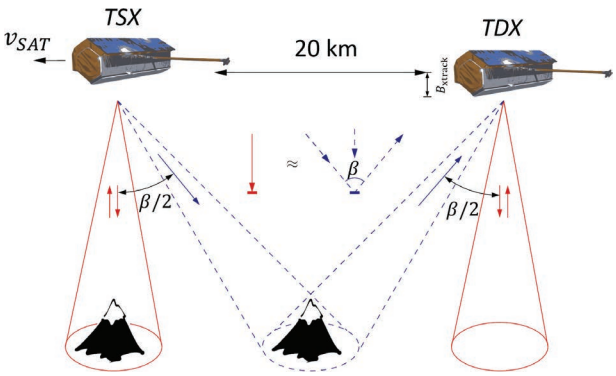

FIGURE 25. The basic configuration of the *TerraSAR-X* (*TSX*) and *TanDEM-X* (*TDX*) satellites in the monostatic commissioning phase, in which the first bistatic SAR acquisitions were performed. The red cones correspond to the natural zero-Doppler beams, whereas the blue cones correspond to the beams used in the bistatic acquisitions.

were processed with the experimental TanDEM-X interferometric processor, developed at the DLR Microwaves and Radar Institute [80]. It is a versatile processing chain for SAR data, including SAR focusing, interferometry, tomography, and time-series analysis. This tool has been expanded and improved through the lifetime of the TanDEM-X mission in order to accommodate the needs of different experiments.

FIRST BISTATIC SPACEBORNE SYNTHETIC APERTURE RADAR IMAGE

The first bistatic acquisitions were conducted in midsummer 2010, with both satellites in pursuit-monostatic configuration, while TanDEM-X underwent its monostatic commissioning phase [81]. As depicted in Figure 25, the spacecraft were separated by about 20 km, which required squinting the beams to ensure footprint overlap, as shown by the blue-dashed cones in the figure. In the figure, the red cones correspond to the natural zero-Doppler beams used in the commissioning phase, whereas the blue-dashed cones correspond to the beams used in the bistatic acquisitions, showing squints of about 2.2°.

Figure 26(a) displays the first bistatic SAR image of TanDEM-X, showing the airplane-shaped metropolitan area of the Brazilian capital and surrounding areas. The image shows in yellow tones structured (e.g., human-made) areas and in gray tones more homogeneous (e.g., natural) areas. The radar illumination came from the left, covering an area of several tens of kilometers in both range and azimuth. Figure 26(b) is an overlay of the bistatic and monostatic images. One can observe a different scattering response despite the small bistatic angle of only 1.6°. For example, the city area shows a dominant monostatic scattering mechanism, whereas some building areas near the lake show a stronger bistatic response. The different sensitivity to the scattering and/or dielectric properties of the scene is just one of the many possibilities offered by bistatic acquisitions.

Shortly afterward, the first bistatic interferometric acquisitions were made, for which pulse-to-pulse toggling between the red and blue beams of Figure 25 was necessary. On top of this, the operation of the *TanDEM-X* satellite in the toggled transmitter/receiver-only mode was affected, which resulted in the simultaneous acquisition of two monostatic and one bistatic images, all with interferometric consistency, in a dual-baseline scenario, which allowed for the derivation of the first bistatic topographic maps of the mission. The toggling of the beams required the use of a high pulse-repetition frequency (PRF), resulting in narrow swaths. The first bistatic interferometric acquisitions were conducted over the Parque Nacional del Volcan Turrialba, in Costa Rica. Figure 27 presents the DEM derived from the first bistatic interferogram of TanDEM-X, overlaid with the interferometric fringes corresponding to the bistatic half baseline.

The image in Figure 27 gives an elevated perspective over the geocoded DEM (along track in the horizontal dimension), showing the top of the volcano around the center–middle-right part of the image. One curiosity of the first bistatic interferometric acquisitions is that the DEMs were computed in the absence of data from the synchronization

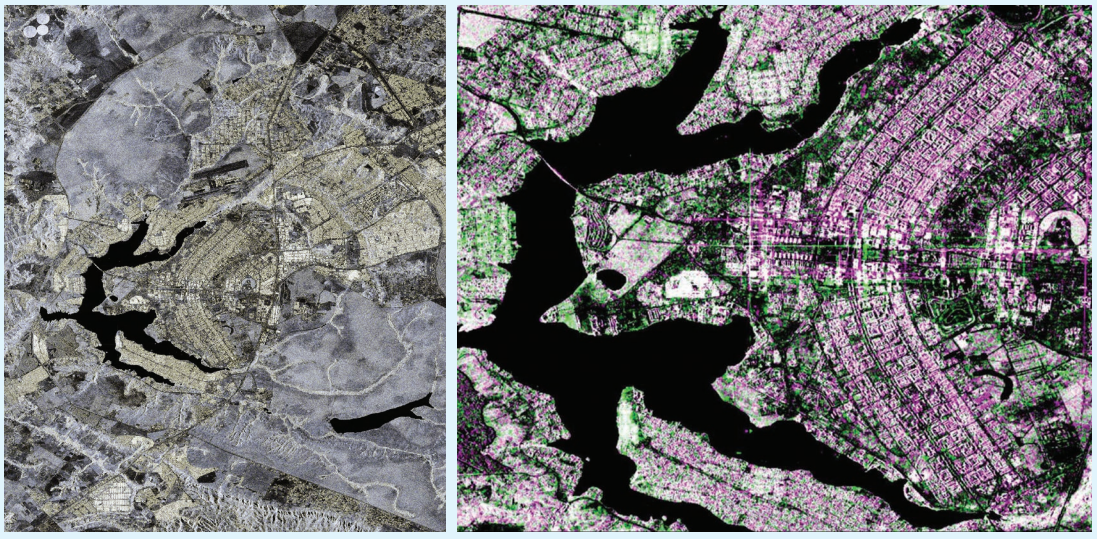

FIGURE 26. (a) The first bistatic SAR image acquired by *TanDEM-X* in summer 2010, over Brasilia, Brazil. The colors represent the structure in the image, with human-made areas appearing in yellow and natural areas appearing in gray. (b) A close-up around the city of Brasilia, showing an overlay of the *TanDEM-X* bistatic image and the *TerraSAR-X* monostatic image in green and magenta, respectively.

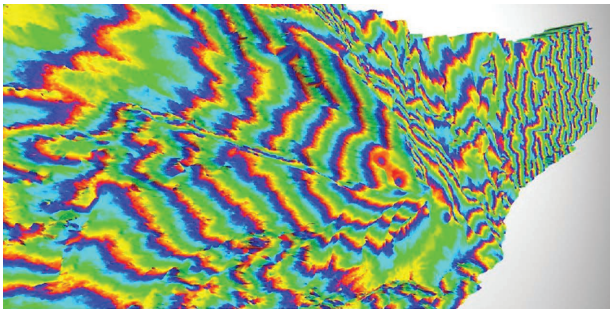

FIGURE 27. The interferometric phase overlaid on the DEM derived from the first bistatic interferometric acquisition of *TanDEM-X* over Parque Nacional del Volcan Turrialba, in Costa Rica.

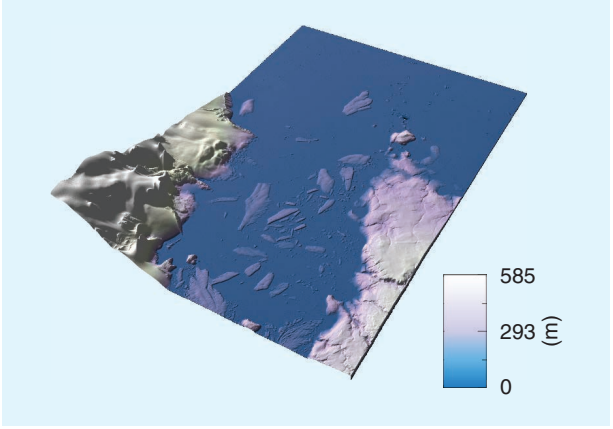

FIGURE 28. The perspective view of the first TanDEM-X DEM acquired with a crossing-orbit configuration in the monostatic mode over October Revolution Island, Russia, on 16 July 2010.

link between the spacecraft, hence relying on the data-based synchronization approach AutoSync [81], showing an early example of synchronization strategies applicable nowadays to partially cooperative bistatic SAR systems and concepts, such as the European Space Agency's (ESA's) Earth Explorer mission Harmony.

FIRST TanDEM-X DIGITAL ELEVATION MODEL

The first DEM produced with data acquired by the *TerraSAR-X* and *TanDEM-X* satellites was created shortly after the launch of the latter, when the satellites were not yet flying in close formation [82]. At that time, the satellites were separated by a large along-track distance such that appropriate interferometric acquisitions were feasible only at high latitudes. Such a configuration resulted in a crossing angle of the ground tracks, which could be compensated by acquiring the two monostatic images under different squint angles. The very large perpendicular baseline of 2 km resulted in an extremely accurate DEM, with a relative vertical accuracy better than 20 cm, which allowed the observation of fine features over the ice, as in Figure 28. Further crossing-orbit experiments have been performed with *TerraSAR-X* and *TanDEM-X* over Antarctica in order to achieve temporal baselines of one, five, and six days in addition to the 11-day repeat [83].

SUPERRESOLUTION

A demonstration of superresolution imaging with *TerraSAR-X* and *TanDEM-X* in order to improve spatial resolution is given in [84], whereby acquisitions were performed during the pursuit-monostatic phase. The idea is to command different center frequencies and/or different squint angles for each satellite such that the two resulting images are processed—with the goal to align the images and remove the impact of the spatial baseline—and then coherently combined in

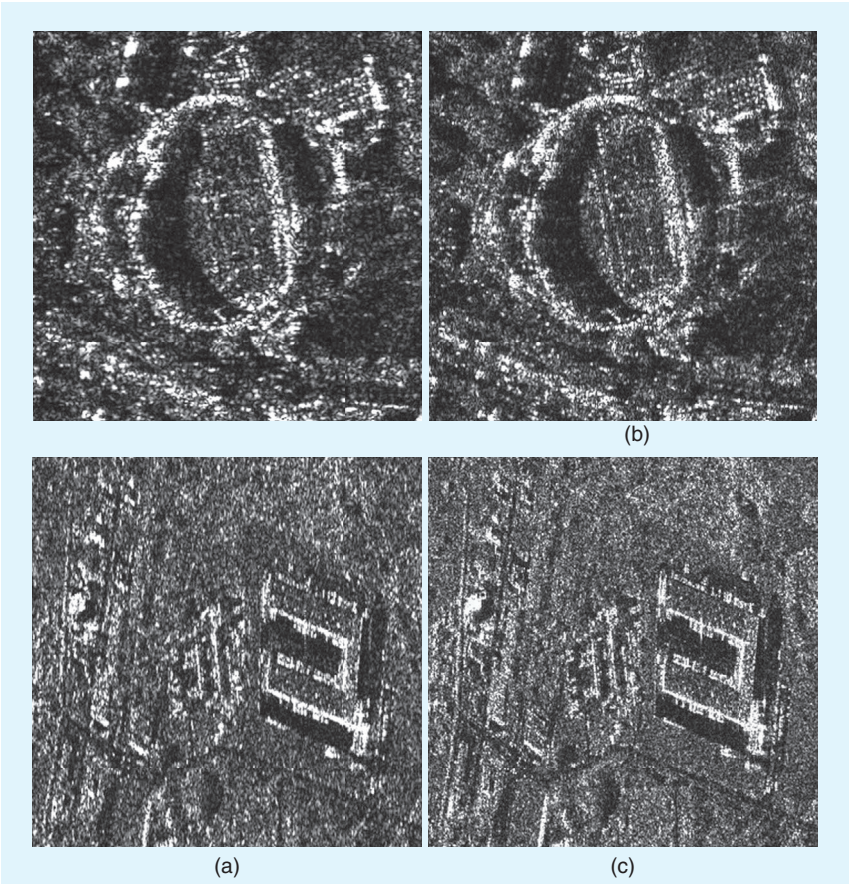

FIGURE 29. A demonstration of superresolution imaging with *TerraSAR-X* and *TanDEM-X*. (a) Single-channel images and resolution-improved products in the (b) range and (c) azimuth. The range is horizontal, and the azimuth is vertical.

order to retrieve a product with twice the spatial resolution. Figure 29 (top) shows an example of a stripmap image with enhanced range resolution over Sydney, NSW, Australia, with a final range resolution of 300 MHz by combining two images with 150-MHz bandwidth each. Figure 29 (bottom) consists of stripmap images with enhanced azimuth resolution over Neustrelitz, Germany, with a final azimuth resolution of 1.5 m after combining the adjacent Doppler spectra. In this latter case, the satellites were commanded to perform monostatic acquisitions with 0 and 0.32°, respectively, in order to obtain contiguous Doppler spectra and achieve a stripmap image with an azimuth spatial resolution factor of two or better.

QUAD-POLARIMETRIC SYNTHESIS

The synthesis of quad-pol images by combining interferometric dual-pol data acquired by *TerraSAR-X* and *TanDEM-X* was suggested in [84], based on airborne experiments performed by the DLR [85]. In this experiment, each satellite received one cross-polar and one copolar channel, and, similar to the superresolution experiment, the data had to be processed coherently in order to remove the impact of the spatial baseline and generate the quad-pol product [84], [86]. *TerraSAR-X* offers quad-pol products only experimentally and with the limitation inherent to the DRA mode, i.e., a lower signal-to-noise ratio and worse azimuth ambiguities. Figure 30 illustrates the Pauli decomposition of a portion of the acquisitions over the Pinyon Pines test site for fully polarimetric images for the DRA mode and the quad-pol synthesis mode. The images show a similar polarimetric signature, where the only relevant effect to be observed is the fact that the image obtained with the DRA mode has more accentuated azimuth ambiguities, which are visible in some parts of the image (e.g., the top right, appearing mainly as double-bounce responses in red around the bluish image area). Further analyses of this experimental mode can be found in [18].

DISTRIBUTED SYNTHETIC APERTURE RADAR SIGNAL RECONSTRUCTION

The first spaceborne demonstration of azimuth SAR signal reconstruction was performed on monostatic *TerraSAR-X* data (DRA mode) acquired before the launch of *TanDEM-X* [88], [89]. The availability of the second satellite enabled the demonstration of distributed SAR imaging using *TerraSAR-X* and *TanDEM-X* data [90], [91]. By combining the data of two or even four phase centers displaced in the azimuth direction, the reconstruction of single high-resolution SAR images with a low azimuth ambiguity-to-signal ratio (AASR) is possible.

Figure 31(a) is a *TerraSAR-X* image over Antarctica, acquired in 2014, with severe azimuth ambiguities highlighted in yellow ellipses. Commands were adjusted to provoke those ambiguities, which subsequently could be mitigated by combining *TerraSAR-X* and *TanDEM-X* data, as in Figure 31(b). This experiment can be regarded as an important step on the way toward a distributed satellite system enabling high-resolution wide swath SAR imaging, providing interferometric and possibly tomographic capabilities at the same time [92], [93].

COHERENT AZIMUTH AMBIGUITIES

TanDEM-X allowed observing for the first time the coherent effect of azimuth ambiguities in SAR interferometry. Among others, the data set acquired on 30 December 2010 over Franz Josef Land, Russia, showed that azimuth

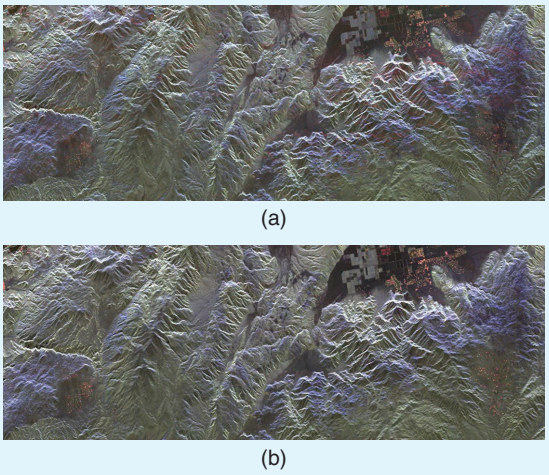

FIGURE 30. A quad-pol synthesis demonstration with *TerraSAR-X* and *TanDEM-X* over the Pinyon Pines test site. (a) The DRA mode. (b) One copolarization and one cross-polarization channel in each satellite. The reflectivity images are represented using Pauli decomposition, where the colors correspond to (red: even bounce) HH – VV, (green: volume scattering) HV + VH, and (blue: odd scattering) HH + VV. Both images show a similar polarimetric response in all areas, whereby the DRA image is more prone to azimuth ambiguities (e.g., at the top right, appearing in red around the bluish image area) due to the wider azimuth antenna beamwidth on receive.

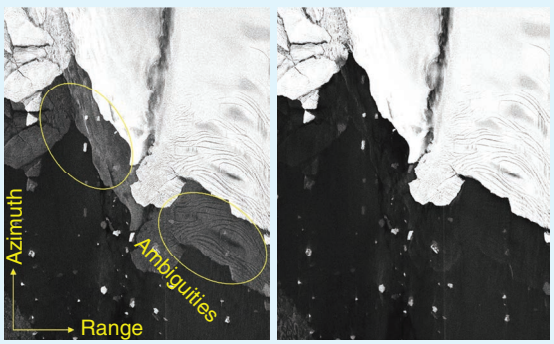

FIGURE 31. Azimuth ambiguity reduction by exploiting multiple phase centers on two satellites, demonstrated over Antarctica. (a) The dominant azimuth ambiguities of the ice shelf in the open-water area, based on a single channel (*TerraSAR-X*). (b) The ambiguities are suppressed by combining the data of *TerraSAR-X* and *TanDEM-X*.

ambiguities can be coherent between the primary and secondary acquisitions and lead to significant biases in the interferometric phases and modulations of the coherence magnitude, with visible artifacts in the resulting DEM. Figure 32(a) is a portion of the interferogram, in which the azimuth ambiguities of the mountain in the lower part of the image are seen in the upper part as a bias in the sea ice region.

Based on these observations, a theoretical model for the coherent effect of ambiguities was developed, which can be used for the design of InSAR systems [94], [95]. Moreover, strategies have recently been proposed to coherently remove azimuth ambiguities through a postprocessing step or to decorrelate them through a slight variation of the pulse repetition interval [96], [97]. The simulation in Figure 32(b) shows that for the same AASR and partially decorrelated ambiguities (coherence of the ambiguity = 0.3), the artifacts become far less visible.

ROTATION OF SEA ICE FLOES

During the monostatic commissioning phase, unique interferometric data sets with very short temporal baselines could be recorded, allowing for the first time the observation of sea ice dynamics. Figure 33(a) is an along-track interferogram obtained in ScanSAR mode near the east coast of Greenland. The interferometric phase reveals cyclic fringe patterns along the azimuth specific to individual ice floes, while areas of land topography produce a less regular phase pattern with smaller variations. The cyclic patterns of the ice floes, which typically have a rather flat topography, are due to rotation about their vertical axes, whereas rather stable ice floes are characterized by small constant phase offsets due to large-scale movement. The fringe pattern can be translated into a measure of horizontal rotation with very high accuracy. Figure 33(b) shows such a rotation map, where the color scale represents rotations between −0.005° (yellow to red) and +0.005° (blue to violet), which occurred within the 3-s separation of the two acquisitions. In addition, estimates of instantaneous ice floe drift can be obtained from the cross correlation of the two images, as described in [98].

LARGE-BASELINE INTERFEROMETRIC SYNTHETIC APERTURE RADAR FOR PRECISE TOPOGRAPHIC MAPPING

During the mission science phase, taking place from October 2014 to December 2015, bistatic acquisitions with across-track baselines up to 3.6 km were acquired. This provided the opportunity to retrieve DEMs with unprecedented vertical accuracy. Special effort was put into in the interferometric processing, due to the small heights of ambiguity and the impact of volume decorrelation. This research resulted in a novel dual-baseline region-growing algorithm for phase unwrapping, which exploits two single-pass interferograms acquired with large baselines [99]. Figure 34 examines the results of an experiment performed over the Atacama Plateau, Argentina. Two interferograms with baselines of 1,178 m (a height of ambiguity of 6.9 m) and 1,432 m (a height of ambiguity of 3.15 m) were used. The bistatic acquisitions took place with a one-month difference. Figure 34 provides a comparison to the TanDEM-X DEM in order to emphasize the better performance in noise reduction of the large-baseline experiment. By comparing the DEMs to a common reference, the TanDEM-X DEM shows a standard deviation of 51 cm, whereas the experimental DEM has a value of

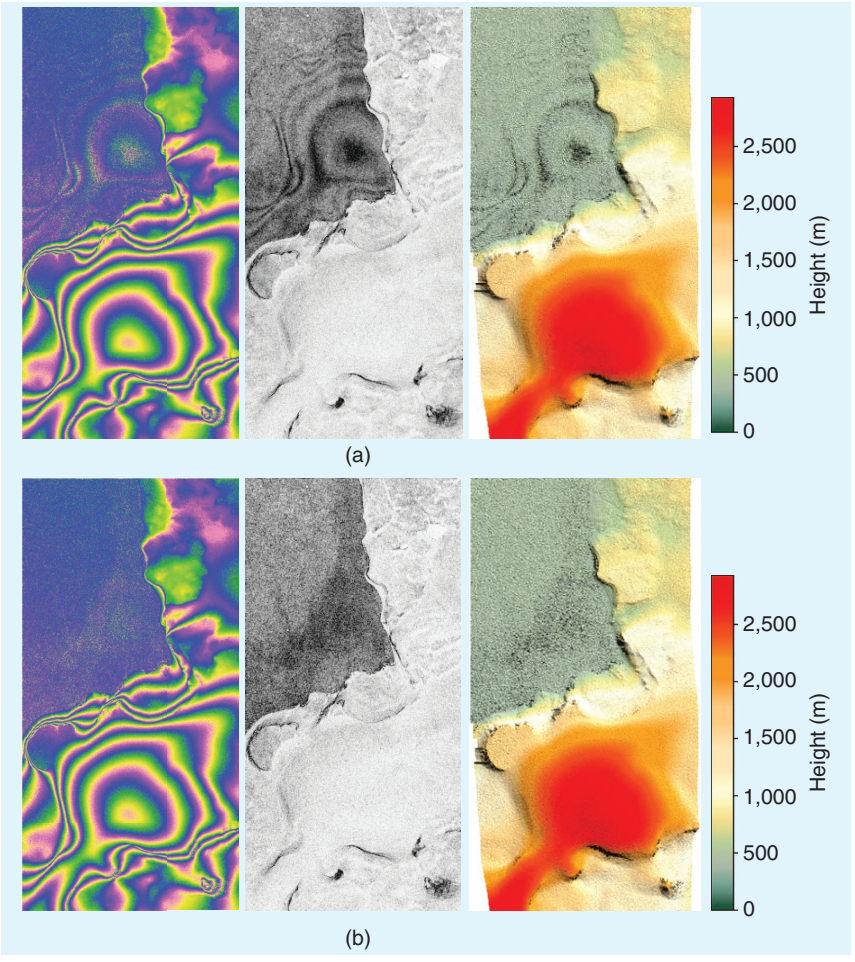

FIGURE 32. (a) The interferometric phase (left), magnitude of the complex coherence (center), and DEM (right) of a detail of a *TanDEM-X* interferogram affected by azimuth ambiguities, acquired over Franz Josef Land. The horizontal and vertical axes represent the ground range and azimuth, respectively. The azimuth ambiguities of the mountain in the lower part of the image are seen in the upper part as a bias in the sea ice region. (b) The simulated interferometric phase (left), magnitude of the complex coherence (center), and DEM (right) for the same AASR and partially decorrelated ambiguities (coherence of the ambiguity = 0.3). The artifacts of the azimuth ambiguities become far less visible. (Adapted from [97].)

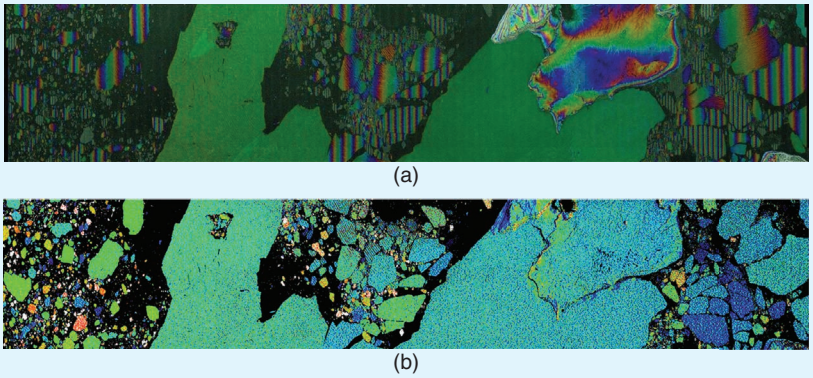

FIGURE 33. (a) An interferogram of rotating ice floes (the blue–red color bar is scaled from $-\pi$ to π). (b) The rotation angle of individual ice floes; the angular range of the measurements corresponds to a colored scale representing a rotation angle from –0.005° (yellow to red) to +0.005° (blue to violet).

27 cm, hence demonstrating the good performance of the approach. Note that in this particular case, the TanDEM-X DEM was produced using two to three coverages, which results in an improvement factor of about 1.4–1.5 in terms of noise reduction, whereas the experimental DEM was obtained with a single coverage.

SYNTHETIC APERTURE RADAR RAW DATA QUANTIZATION

Efficient SAR raw data quantization represents an aspect of utmost importance for present and next-generation SAR systems, which will require the acquisition of a large volume of data. The flexibility offered by the TanDEM-X system allowed for the assessment of raw data compression in SAR and interferometric data. For this purpose, several experimental bistatic acquisitions have been commanded, with full compression (8-bit analog-to-digital converter) in both *TerraSAR-X* and *TanDEM-X* SAR instruments. The recorded SAR raw data were compressed on the ground into multiple data sets using all available block-adaptive quantization rates. The obtained raw data products were then processed into SAR images, from which interferograms, coherence maps, and DEMs were derived. This data set represents the basis for the detailed assessment of quantization effects in TanDEM-X data [100], together with the demonstration of noninteger compression rates [101], also in the frame of performance-optimized quantization exploiting a priori information of SAR backscatter [102]. The implementation of a method for efficient data rate allocation for the joint optimization of resource allocation and resulting performance degradation based on DL was introduced in [103]. Figure 35(a) shows a SAR backscatter map over the urban area of Mexico City, Mexico, acquired by *TanDEM-X*, while Figure 35(b) depicts the bitrate map derived according to the approach proposed in [103] to achieve a target signal-to-quantization noise ratio (SQNR) of 15 dB.

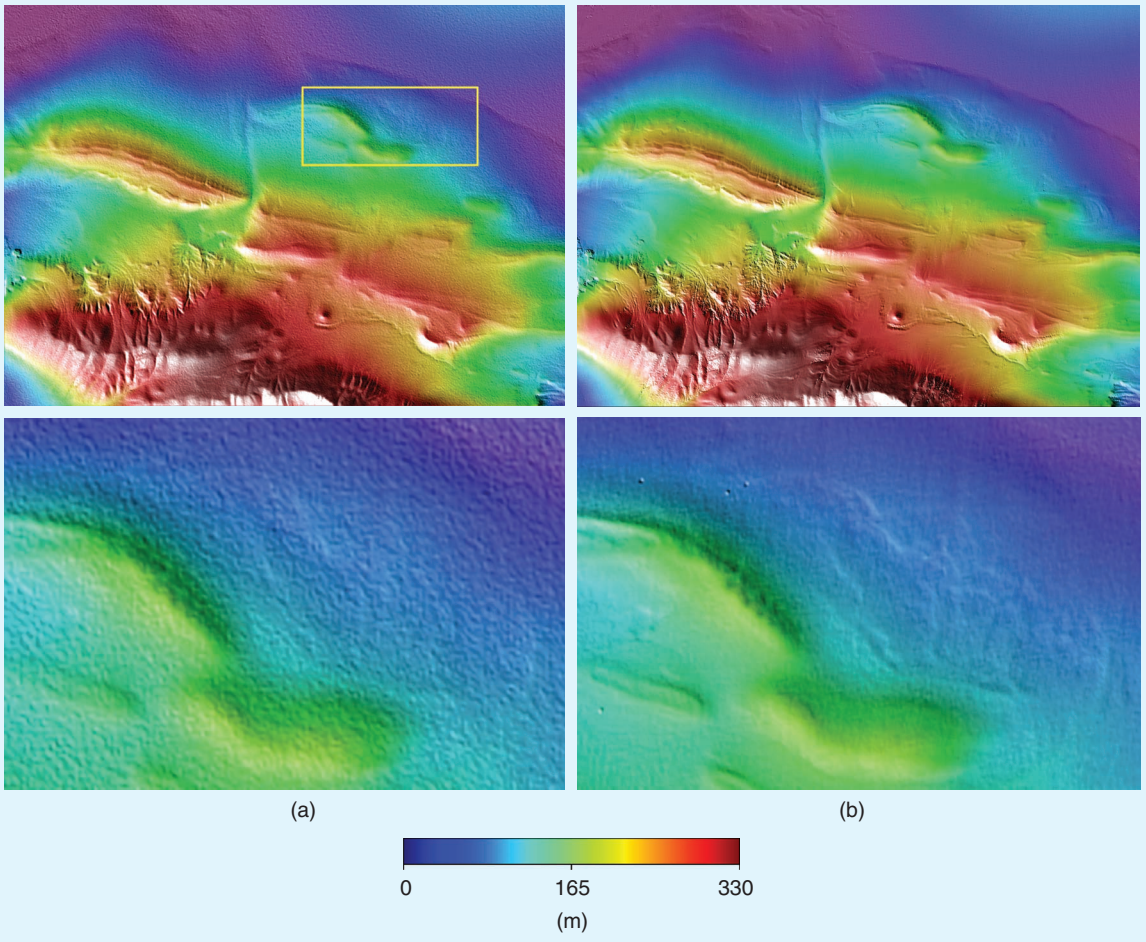

FIGURE 34. A large-baseline experiment over the Atacama Plateau, Argentina. (a) The global TanDEM-X DEM as a reference. (b) The result of the large-baseline experiment. The second row is a close-up of the first image, indicated by the yellow rectangle in the first image, which clearly shows the noise reduction improvement of the large-baseline experiment.

The resulting SQNR map appears in Figure 35(c), demonstrating the effectiveness of the method (a rather homogeneous distribution of SQNR values is observed).

DETECTION OF MARITIME AND LAND MOVING TARGETS

The *TerraSAR-X/TanDEM-X* satellite formation is well suited for detecting maritime and land moving targets, especially if it is operated in the pursuit-monostatic mode with a large along-track baseline on the order of several kilometers [104]. The actual geographical positions of a moving target and the velocities and moving directions can be estimated with high accuracy.

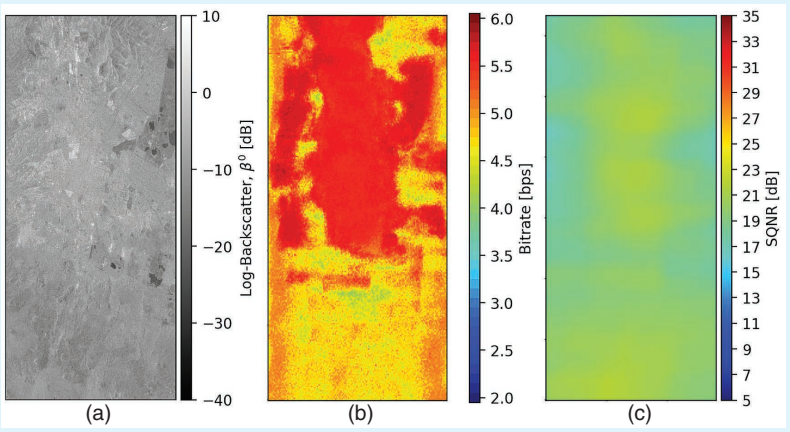

FIGURE 35. The (a) SAR backscatter map acquired by *TanDEM-X* over the urban area of Mexico City, Mexico; (b) bitrate map derived according to the method in [27] to achieve a target signal-to-quantization noise ratio (SQNR) of 20 dB; and (c) resulting SQNR map.

The moving target is observed by both platforms at different times. In each of the focused radar images, the target may appear several hundred meters displaced from its actual geographical position. For instance, for an *X*-band spaceborne system in low-Earth orbit, the azimuth displacements of ships can be in the order of 600 m and for fast moving

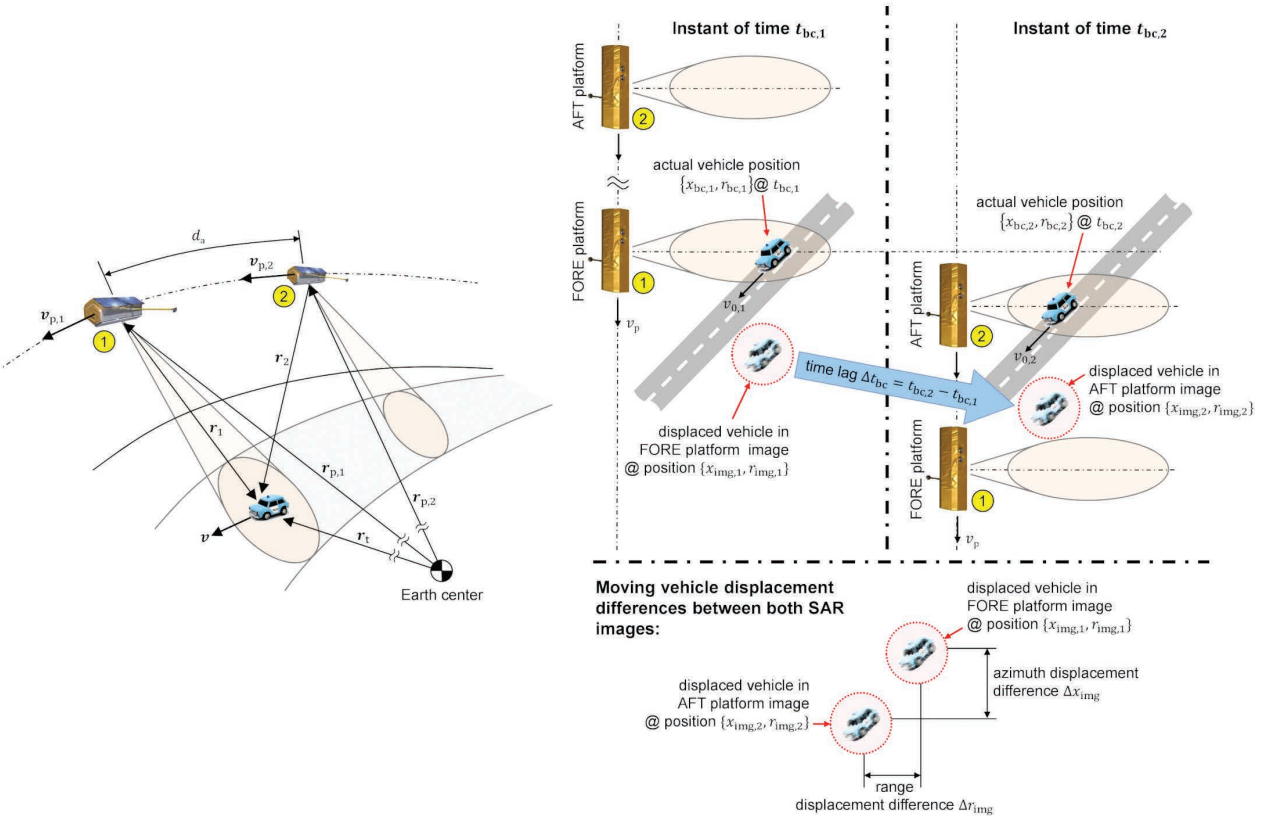

FIGURE 36. The (a) spaceborne dual-platform acquisition geometry and (b) moving target displacements in each of the two images as well as the range and azimuth displacement differences [104].

land vehicles, up to 2,000 m and more. By measuring the range and azimuth displacement differences of the detected targets between both radar images [see Figure 36(b)], the actual geographical positions of land and maritime moving targets, the absolute velocities, and the moving directions can be computed unambiguously with high accuracies.

For automatically measuring the displacement differences, a 2D cross correlation carried out on a subpixel basis is used. For extended objects occupying more than a single resolution cell, as is usually the case for larger ships, a potential target rotation is considered by the implemented 2D correlator [103].

Figure 37 provides a ship detection example over the Strait of Gibraltar. The detected ships are depicted as colored symbols on their estimated actual positions. The color corresponds to the estimated velocity.

For the *TerraSAR-X/TanDEM-X* formation in pursuit-monostatic mode, with a temporal along-track separation of 2.5 s, the achieved and verified position accuracy is on the order of 11 m, the absolute velocity accuracy is better than 1 km/h, and the moving direction accuracy is 0.55°. Such accuracies allow for precise prediction of the future target position, which is important for security applications. With a single spacecraft, even if it is carrying a powerful multichannel SAR system, such accuracies are generally not reachable, mainly due to the very limited along-track baselines available on a single spacecraft.

SYNTHETIC APERTURE RADAR TOMOGRAPHY: FOREST

SAR tomography is emerging as a revolutionary technique for future spaceborne missions. It allows one to retrieve the 3D structure of intricate volumetric scatterers like forests and ice, where multiple contributions occupy in layover the same resolution cell, [105], [106].

However, a major obstacle lies in temporal decorrelation since changes among data acquisitions can distort the final image. To combat this, interest in designing missions with multiple radar sensors operating quasi-simultaneously has exponentially grown in recent years. In this context, the TanDEM-X constellation, being the first spaceborne single-pass SAR interferometer in formation flight, has already provided a first demonstration of tomographic imaging over forested areas. In particular, coherent mapping based on the Van Cittert–Zernike theorem, which offers a partial solution to the temporal decorrelation problem, can be exploited [107]. This approach relies on a set of single-pass interferometric coherences acquired at nearly the same time. Preliminary results of coherence-based tomography have been shown in [108]. The limited tomographic resolution of the prescience phase of TanDEM-X hinders a full demonstration of the technique's potential. However, the beginning of the TanDEM-X science phase has provided invaluable data in several fields and allowed developing and analyzing coherence-based tomography [109]. As an example, to demonstrate the tomographic capabilities, data were

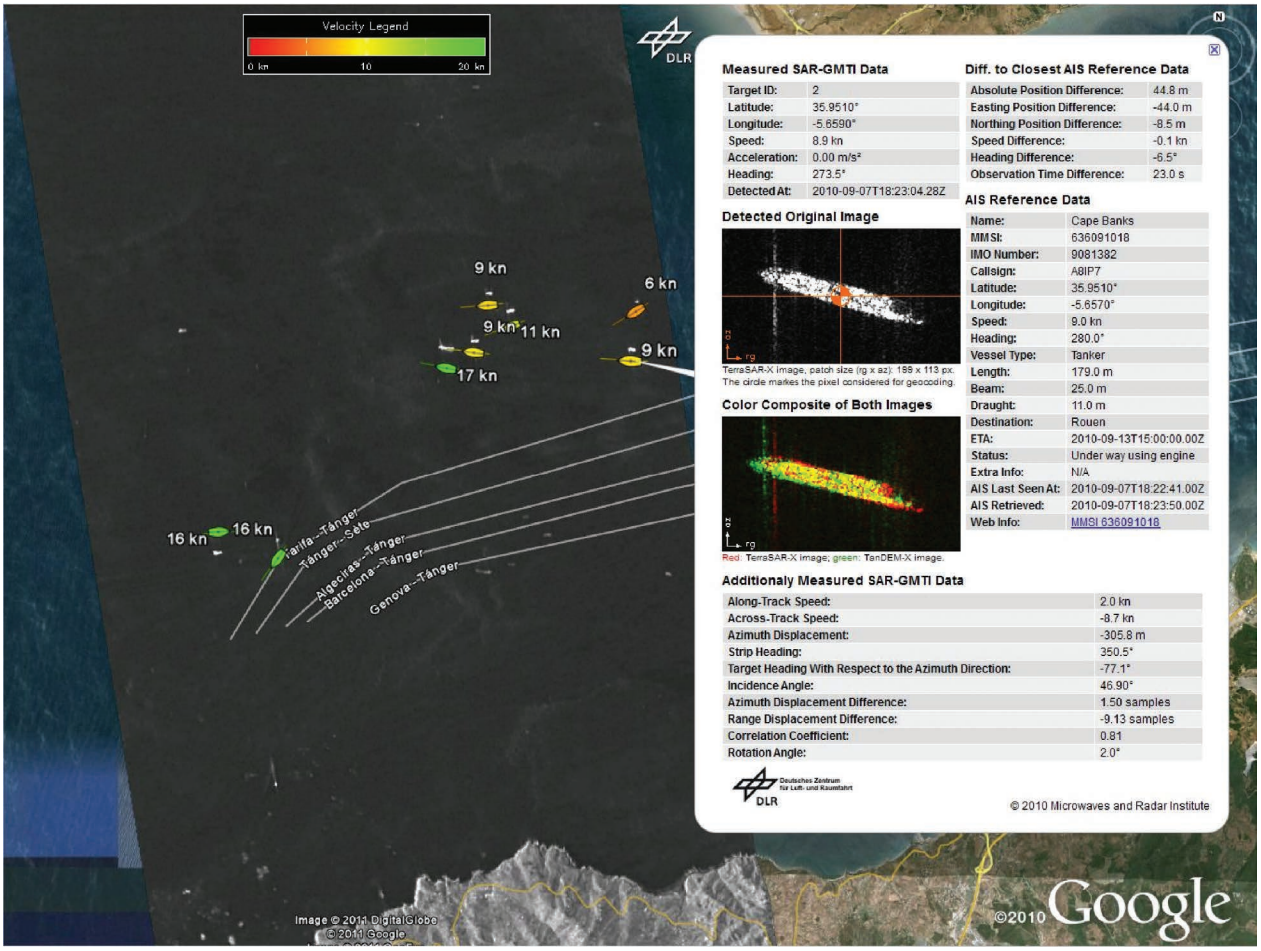

FIGURE 37. A Google Earth image of the Strait of Gibraltar overlaid with a *TerraSAR-X* radar image and color-coded symbols representing the actual geographical positions of detected ships. The popup window on the right shows the estimation details of a particular ship, including the differences to the automatic identification system (AIS) ground truth data.

acquired with *TanDEM-X* over boreal forests. As shown in Figure 38, it is possible to retrieve volumetric information of forests by exploiting data in the quasi-monostatic acquisition mode and processing with coherence-based tomography. As a reference, a tomogram obtained with the Capon superresolution method [110] is also reported, showing that both coherence-based and Capon methods rely on the same interferometric information. As can be observed due to the sparse nature of forests, it is possible to clearly retrieve contributions from both the ground and the canopy.

TanDEM-X has demonstrated the feasibility of spaceborne SAR tomography for volumetric targets like forests at the *X* band. Analysis of the retrieved data using coherence-based tomography highlights their crucial role in equipping future space missions to address upcoming challenges.

BIDIRECTIONAL SYNTHETIC APERTURE RADAR IMAGING

A further experimental imaging mode that was demonstrated with TanDEM-X is the bidirectional SAR (BiDiSAR) imaging mode [111]. It allows for simultaneous imaging in two or more directions using only one antenna and one receiving channel, and by this, it enables the acquisition of short-term time series of images and interferograms with different squint angles. The underlying principle lies in the exploitation of grating lobes that arise in array antennas for large steering angles in combination with a PRF selection that separates the spectra of the different directions.

The example in Figure 39 presents a short time series of interferograms of the Upsala Glacier that was acquired with the *TerraSAR-X* and *TanDEM-X* satellites in the pursuit-monostatic configuration. The forward and backward images were obtained by steering the main lobe by 2.2° in the azimuth direction, which caused a grating lobe at –2.2°, with the same array factor as the main lobe. Figure 39(b) was acquired by an interleaved acquisition block with the boresight antenna beam, i.e., a steering angle of 0°. In the pursuit-monostatic mode, such an acquisition scheme could be exploited to measure surface currents or sea ice velocities since the different squints are sensitive to different projections of the motion vector, hence allowing the retrieval of 2D velocity fields (see the "Bistatic Bidirectional Synthetic Aperture Radar for Ocean Applications" section).

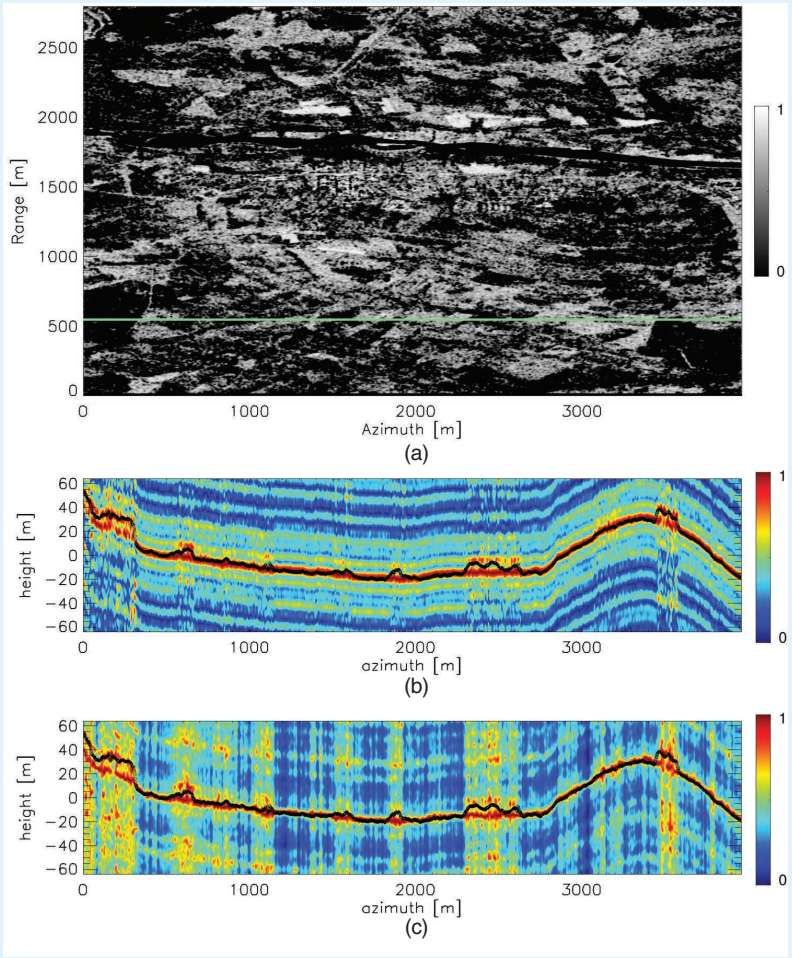

FIGURE 38. A tomographic reconstruction over boreal forest by means of *TanDEM-X* data. (a) The region of interest near the village of Vindeln, Sweden. The green line depicts the considered profile. (b) A coherence-based tomogram. (c) A Capon superresolution tomogram based on single-look complex images.

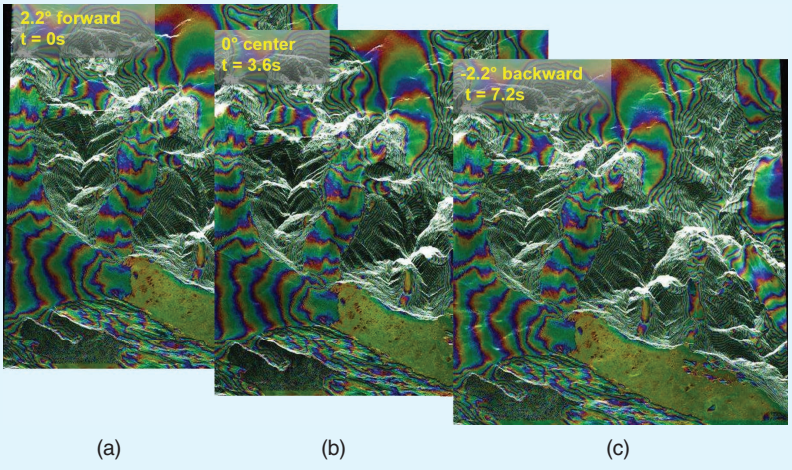

FIGURE 39. A short-term interferogram time series of the Upsala Glacier acquired by a combination of bidirectional and boresight antenna steering.

It can also be used to increase the number of acquisitions for the detection and velocity measurement of ground and maritime moving targets (see Section "Detection of Maritime and Land Moving Targets" and [94]).

BISTATIC BIDIRECTIONAL SYNTHETIC APERTURE RADAR FOR OCEAN APPLICATIONS

Another experiment with BiDiSAR was performed in the bistatic mode in order to retrieve 2D wind and total surface current vectors [39] as a testbed for potential future missions addressing ocean applications, like the ESA's Earth Explorer 10 Harmony mission [39]. In this case, the two satellites were flying in close formation with an almost-zero cross-track baseline and an along-track baseline of about 50 m, hence having an optimum configuration to perform ATI by combining the images acquired by the two satellites. In the BiDiSAR mode, the corresponding fore and aft images were combined to obtain the fore and aft along-track interferograms. Figure 40 gives the obtained results over the tip of Novaya Zemlya, Russia [87]. These results demonstrate the potential to obtain high-resolution characteristics of upper-ocean dynamics by exploiting InSAR data acquired with azimuth angular diversity.

CONCLUSIONS AND LESSONS LEARNED

The TanDEM-X mission is a unique mission with 3D-to-4D data acquisition capability and is currently delivering invaluable data for operational, science, and experimental information products. This is possible only due to the highly reconfigurable and flexible mission concept, which was one of the main requirements for the implementation of the bistatic mission. New and innovative applications were developed and demonstrated based on the capabilities provided by *TanDEM-X*. The main highlights of the TanDEM-X mission are summarized in the following.

One of the major achievements of the TanDEM-X mission is that the TanDEM-X DEM became a standard for geospatial applications and is today the basis for the Copernicus DEM for a variety of scientific applications, while WorldDEM is widely used for a variety of commercial applications.

The bistatic SAR mission concept in close-formation flight was in 2010 far beyond the state of the art in spaceborne SAR and is the only operational bistatic single-pass interferometric mission in space to date. Furthermore, TanDEM-X was the first radar mission to demonstrate innovative imaging modes (superresolution, a large across-track baseline mode, an along-track baseline mode, polarimetric SAR interferometry, tomography, double differential SAR interferometry, the Terrain Observation by Progressive Scans (TOPS) mode now implemented on *Sentinel-1*, and so on).

The immense interest of the scientific community, with approximately 6,500 registered principal investigators on the TanDEM-X science server, is by far greater than expected. TanDEM-X continues to provide unique bistatic data even after 14 years of mission operation. The main feature is the innovative mission concept and interferometric data provision with three data request streams: operational DEM products, selected science products with orders on demand, and experimental products with demonstration character.

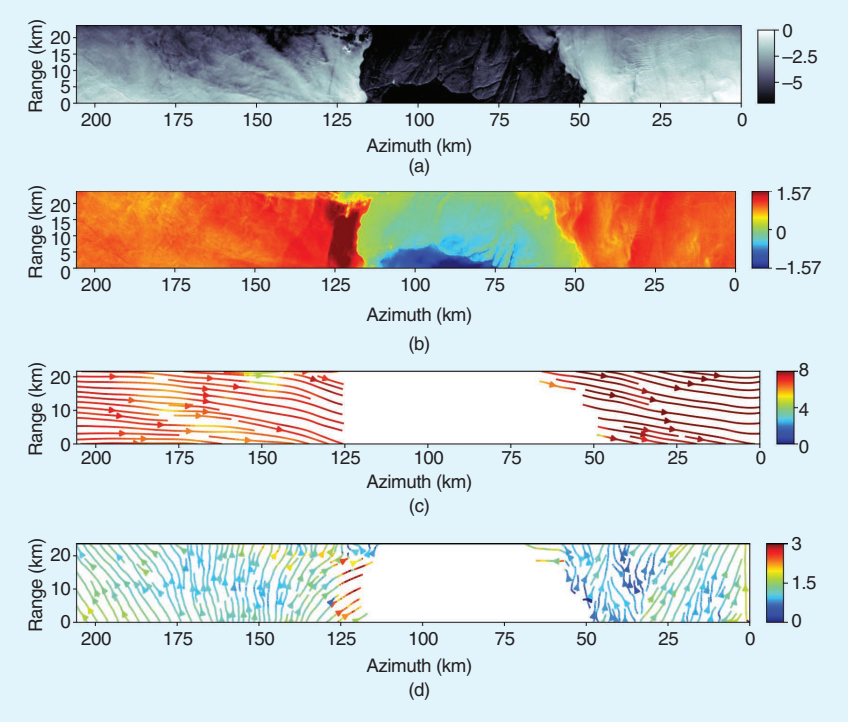

FIGURE 40. An experimental bistatic BiDiSAR demonstration for the retrieval of wind and total surface current vectors over Novaya Zemlya, Russia. The (a) normalized radar cross section (in decibels), (b) aft interferogram (in radians), (c) retrieved wind field at a roughly 10-km resolution (in meters per second), and (d) retrieved total surface current vector at a 250-m resolution (in meters per second).

Several new information products have been generated from the TanDEM-X data sets, which were not foreseen before: the DCMs, forest/nonforest global map, HydroSHEDS, water mask, EDEM, global urban footprint, coastline map, and so on.

The DEM editing is a challenging task, depending on the required level of accuracy. Many new algorithms have been developed for the TanDEM-X 30-m DEM edited version, and further developments will significantly improve the EDEM. In a next step, artificial intelligence methods will also play an important role in improving the DEM editing quality.

The 4D data (i.e., DEM time series) became, in the course of the mission, much more important than expected. Due to the fast-changing processes on Earth's surface, some of which are triggered by global warming, a new TanDEM-X mission phase was established in 2022, the so-called 4D mission phase, which will continue in the coming years.

At the last TanDEM-X science team meeting, in October 2023, in Oberpfaffenhofen, we received demanding requests for the generation of a new and improved DEM data set that will drive a follow-on mission(s) to TanDEM-X:

- There is a request for a global DEM with similar height accuracy (i.e., with a relative height accuracy of 2 m, with a 90% confidence interval) but with 4-m sampling in order to keep pace with the spatial resolution improvement of future remote sensing sensors. For example, Sentinel-1 New Generation will provide data with 25-m^2 spatial resolution and a swath width of 400 km.
- There is a need for a continental-scale DEM with decimetric height accuracy for ice/snow/permafrost changes, with 50–100-m posting. This DEM product specification was derived from the science requirements of a mission proposal for permafrost at the Ka band, with a single-pass interferometric formation submitted to previous ESA Earth Explorer calls.
- A need for multibaseline SAR concepts has been identified to fulfill user requirements for improved accuracy and spatial sampling as well as for the robustness of the interferometric processing to solve the phase unwrapping problem. As an example, the MirrorSAR concept was developed, which allows the implementation of multibaseline interferometry with reduced costs and complexity [25].

With the TanDEM-X mission, several challenges associated with bistatic imaging and formation flying have been successfully overcome. The advantage of an increased observation space and the associated increased information space makes bistatic and multistatic mission concepts very attractive. In 2022, the ESA Earth Explorer mission Harmony (C band, with a launch planned for 2029) was selected as the first European multistatic SAR mission. The ESA is also planning a phase 0 study to investigate companion satellite concepts for the Copernicus Radar Observing System for Europe at L-Band mission, and the DLR has started a phase 0 study for an *X*-band follow-on mission to TanDEM-X, considering multibaseline interferometry as an option.

In many ways, the TanDEM-X mission can be regarded as a pioneering radar mission. It paves the way for future bi- and multistatic missions and for innovative 3D and 4D applications.

AUTHOR INFORMATION

Irena Hajnsek (irena.hajnsek@dlr.de) received her diploma degree (with honors) in fluvial river systems from the Free University of Berlin, Berlin, Germany, in 1996 and her Dr. rer. nat. degree (with honors) in model-based estimation of soil moisture from fully polarimetric synthetic aperture radar from the Friedrich Schiller University of Jena, Jena, Germany, in 2001. Since November 2009, she has been a professor of Earth observation at the Swiss Federal Institute of Technology Zürich, Zürich, Switzerland, and the Institute of Environmental Engineering, Zürich, and, at the same time, the head of the Polarimetric SAR Interferometry Research Group, Microwaves and Radar Institute, German Aerospace Center. Since 2010, she has been the science coordinator of the German satellite mission TanDEM-X mission for Digital Elevation Measurement. In 2024 she was awarded a Ph.D. degree honoris causa from the University of Oslo, Norway. She is a Fellow of IEEE.

Thomas Busche (thomas.busche@dlr.de) graduated with his diploma degree in geography from the Georg August University of Göttingen, Germany, in 2000. From 2000 to 2002, he worked in a start-up company as an expert in remote sensing and geographic information systems. From 2003 to 2007, he worked in the Sea Ice Physics group at the Alfred Wegner Institute for Polar and Marine Research, in Bremerhaven, Germany. Since 2007, he has worked at the Institute for Microwaves and Radar, German Aerospace Center, Germany, where he is responsible for the scientific coordination of the TanDEM-X mission.

Sahra Abdullahi (sahra.abdullahi@dlr.de) received her B.Sc. degree in geography from Ludwig-Maximilians-Universität München, Munich, Germany, and her M.Sc. degree (with honors) in geospatial technologies from Technische Universität Graz, Graz, Austria, in 2009 and 2012, respectively. In 2018, she received her Dr. rer. nat. degree (with honors) from the Technical University of Munich. Since 2017, she has been with the German Remote Sensing Data Center, German Aerospace Center, Wessling, Germany, where she is involved in the TanDEM-X for Digital Elevation Measurement PolarDEM framework. Her research focuses on synthetic aperture radar interferometry in the fields of forestry and glaciology.

Markus Bachmann (markus.bachmann@dlr.de) received his Dipl.-Ing. degree in electrical engineering from the Technical University of Karlsruhe, Karlsruhe, Germany, in 2005. In 2005, he joined the Microwaves and Radar Institute, German Aerospace Center. From 2005 to 2011, he was in charge of the implementation and calibration of the *TerraSAR-X*/*TanDEM-X* antenna model. From 2006 to 2010, he assessed the methods and potentials of the digital elevation model calibration for *TanDEM-X*. From 2008 to 2010, he was responsible for the planning and execution of the *TanDEM-X* commissioning phase. In 2011/2012, he performed the interferometric and radargrammetric calibration of the *TanDEM-X* system and established the monitoring of the global coverage for the TanDEM-X mission. Since 2012, he has led the mission engineering group, German Aerospace Center, Germany, with tasks like the acquisition planning and monitoring of the TanDEM-X mission and the assessment of orbit-related issues.

Stefan V. Baumgartner (stefan.naumgartner@dlr.de) received his Dipl.-Ing. (M.S.) degree (with honors) in electrical and communication engineering from the Graz University of Technology, Graz, Austria, in 2004 and his Dr.-Ing. (Ph.D.) degree (with honors) in electrical and communication engineering from the Karlsruhe Institute of Technology, Karlsruhe, Germany, in 2014. Since 2004, he has been with the Microwaves and Radar Institute, German Aerospace Center (DLR), Germany, where he works in the Department of Radar Concepts as a scientist and project manager. Since 2022 he has led a team with research topics related to maritime security and transportation infrastructure monitoring. He was responsible for the first successful bistatic experiment between the DLR's synthetic aperture radar airborne radar sensor and Germany's *TerraSAR-X* radar satellite. Since 2016, he has also been a lecturer at Friedrich-Alexander-University Erlangen, Germany. He is a Senior Member of IEEE.

Allan Bojarski (allan.bojarski@dlr.de) received his Dipl.-Ing. degree in aerospace engineering from the Technical University of Munich, Germany, in 2014. After two years performing battery simulations for the Daimler R&D department, in Ulm, Germany, in 2016, he joined the Microwaves and Radar Institute, German Aerospace Center, Oberpfaffenhofen, Germany. He is currently involved in various spaceborne synthetic aperture radar (SAR) projects as a mission engineer. In this context, he is responsible for the long-term system monitoring of the *TerraSAR-X*/*TanDEM-X* satellites and the scientific acquisition planning for the TanDEM-X mission. Furthermore, he designs mission scenarios, SAR satellite formations, and observation concepts for several SAR missions, such as Tandem-L or High Resolution Wide Swath.

Jose-Luis Bueso-Bello (jose-luis.bueso-bello@dlr.de) received his Ingeniero degree in telecommunications engineering from the Universidad Politécnica de Valencia, Spain, in 2003 and his M.Sc. degree in Earth-oriented space science and technology from the Technical University of Munich, Germany, in 2007. In 2003, he started working in the Microwaves and Radar Institute, German Aerospace Center, Oberpfaffenhofen, Germany, as a system engineer in the Department of Reconnaissance and Security, where he worked on the definition, design, and analysis for different synthetic aperture radar (SAR) missions. In 2010, he joined the Department of Satellite SAR Systems, where he works as a project engineer, with a focus on the planning, evaluation, and performance monitoring of *TanDEM-X* interferometric SAR acquisitions.

Thomas Esch (thomas.esch@dlr.de) received his diploma degree in applied physical geography from the University of Trier, Germany, in 2003 and his Ph.D. degree (Dr. rer. nat. degree) in geography/remote sensing from the Julius Maximilians Universität of Würzburg, Germany, in 2006. In 2023, he was appointed honorary professor in the Faculty of Geomatics, Computer Science, and Mathematics, University of Applied Sciences Stuttgart, Stuttgart, Germany. He is a German Aerospace Center (DLR) senior scientist and head of the Smart Cities and Spatial Development team at the German Remote Sensing Data Center, Earth Observation Center, DLR, Wessling, Germany.

Thomas Fritz (thomas.fritz@dlr.de) received his diploma degree in physics from the University of Münster, Germany, in 1996 and his Ph.D. degree in astronomy from the University of Bonn, Germany, in 2000. He had a postdoctoral position with the Radioastronomical Institute, University of Bonn. In 2003, he joined the Remote Sensing Technology Institute, German Aerospace Center (DLR), Wessling, Germany, and participated in the development of the *TerraSAR-X* multimode synthetic aperture radar (SAR) processor. In particular, he was responsible for the *TerraSAR-X* SAR product specification and product performance. Since 2008, he has led the development of the operational bistatic interferometric SAR processing chain for the TanDEM-X mission. Currently, he is the leader of the new SAR applications team in the Remote Sensing Technology Institute, DLR, working on digital elevation model (DEM) applications and interferometric SAR/DEM processing chain designs for future SAR missions.

Alberto Alonso-Gonzalez (alberto.alonso-gonzalez@upc.edu) received his B.Sc. degree in computer science, his M.Sc. degree in telecommunication engineering, and his Ph.D. degree from the Technical University of Catalonia (UPC), in 2007, 2009, and 2014, respectively. From 2009 to 2014, he was with the Department of Signal Theory and Communications, UPC. From 2014 to 2022, he was with the Microwaves and Radar Institute, German Aerospace Center, Wessling, Germany, as a member of the Polarimetric SAR Interferometry Research Group. Since 2022, he has been with the Remote Sensing, Antennas, Microwaves, and Superconductivity Group, Department of Signal Theory and Communications, UPC, Barcelona, Spain. He is a Member of IEEE.

Carolina Gonzalez (carolina.gonzalez@dlr.de) received her Ingeniero Civil degree in telecommunication engineering from the Universidad Técnica Federico Santa María, Valparaiso, Chile, in 2004. In 2005 she joined the Microwaves and Radar Institute, German Aerospace Center, Oberpfaffenhofen, Germany, in the System Engineering and Calibration Segment of *TerraSAR-X*, taking care of performance optimization. For the TanDEM-X mission, she worked first in the Instrument Operations and Calibration Segment and later in the Radar Science Group. She covered several aspects of the mission, from system engineering, digital elevation model (DEM) performance, and validation of global products to the production of global 30-m DEM and global change map products. She is a Member of IEEE.

Lanqing Huang (huang@ifu.baug.ethz.ch) was a visiting Ph.D. student and, later, a postdoctoral researcher at the Chair of Earth Observation and Remote Sensing, ETH Zürich, from 2018 to 2023, focusing on retrieving sea ice topography using *TanDEM-X* data. She is currently a postdoctoral fellow at University College London, London, U.K. Her research interests include synthetic aperture radar polarimetry and interferometry, with a focus on marine and cryosphere applications.

Thomas Kraus (t.kraus@dlr.de) received his M.Sc. degree in electrical engineering from the University of Ulm, Ulm, Germany, in 2009. In 2010, he joined the Microwaves and Radar Institute, German Aerospace Center, Wessling, Germany, where he currently works in the field of spaceborne synthetic aperture radar (SAR). He is involved in the instrument commanding, processing, and analysis of scientific and experimental acquisitions in the framework of *TerraSAR-X* and *TanDEM-X*. He was responsible for performance analysis during the operational implementation of the staring spotlight and the wide scanning SAR modes of *TerraSAR-X* as well as the dual-receive antenna mode in the bistatic science phase of *TanDEM-X*. For the geostationary mission proposal HydroTerra, he contributed the SAR performance analysis.

Marie Lachaise (marie.lachaise@dlr.de) received her engineer degree in electronics, telecommunications, and computer science from CPE Lyon, Villeurbanne, France, in 2005; her M.Sc. degree in embedded systems and medical images from INSA Lyon, Villeurbanne, in 2005; and her Ph.D. degree in engineering from the Technical University of Munich, Germany, in 2015. Since 2005, she has been with the German Aerospace Center, Oberpfaffenhofen, Germany. She developed software and algorithms for the TerraSAR-X and TanDEM-X missions. In particular, she designed the algorithms related to the interferometric processing of the multichannel data of the TanDEM-X mission, such as the multibaseline phase unwrapping. Since 2012, she has been responsible for the development and

integration of the enhanced interferometric *TanDEM-X* processor, and since 2016, has been the systems engineer responsible for the change digital elevation model product.

Shiyi Li (shiyi.li@ifu.baug.ethz.ch) received his B.S. degree from Nanjing University in 2014 and his M.S. degree jointly from Delft University of Technology, ETH Zürich, and RWTH Aachen University in 2018. He is currently working toward his Ph.D. degree in environmental engineering at ETH Zürich, Zürich, Switzerland. His research interests include monitoring glacier systems with synthetic aperture radar. He is a Graduate Student Member of IEEE.

Francisco Lopez Dekker (f.lopezdekker@tudelft.nl) was born in Nijmegen, The Netherlands, in 1972. He received his Ingeniero degree in telecommunication engineering from the Universitat Politècnica de Catalunya, Barcelona, Spain, in 1997; his M.S. degree in electrical and computer engineering from the University of California, Irvine, Irvine, CA, USA, in 1998, under the Balsells Fellowship; and his Ph.D. degree from the University of Massachusetts Amherst, Amherst, MA, USA, in 2003. In 2003, he joined Starlab Barcelona. From 2004 to 2006, he was a visiting professor in the Department of Telecommunications and Systems Engineering, Universitat Autònoma de Barcelona. From 2009 to 2016, he led the SAR Missions Group, Microwaves and Radar Institute, German Aerospace Center, Wessling, Germany. Since 2016, he has been an associate professor with the Department of Geoscience and Remote Sensing, Faculty of Civil Engineering and Geosciences, Delft University of Technology, Delft, The Netherlands. He is a Senior Member of IEEE.

Kathrin Maier (maierk@ethz.ch) earned her M.Sc. degree in transport and geoinformation technology from the KTH Royal Institute of Technology, Stockholm, Sweden, in 2017. She is currently a Ph.D. researcher at ETH Zürich, Zürich, Switzerland, focusing on multimodal remote sensing to monitor rapid permafrost thawing and its impact on the permafrost carbon cycle.

Michele Martone (michele.martone@dlr.de) received his B.Sc. and M.Sc. degrees in telecommunication engineering from the University of Naples Federico II, Naples, Italy, in 2006 and 2009, respectively, and his Ph.D. degree from the Karlsruhe Institute of Technology, Karlsruhe, Germany, in 2019. Since 2009, he has been with the Microwaves and Radar Institute, German Aerospace Center, Oberpfaffenhofen, Germany, where he has participated in the development and optimization of the TerraSAR-X and TanDEM-X spaceborne synthetic aperture radar (SAR) missions and the generation of the global *TanDEM-X* digital elevation model and forest/nonforest map and where he has been involved in several projects in collaboration with research and industry partners focused on the design and optimization of future SAR missions. He is a Member of IEEE.

Pietro Milillo (pietro0milillo@gmail.com) received his B.Sc. (laurea) and M.Sc. degrees in physics, with a thesis on synthetic aperture radar and GPS data processing, from the University of Bari, Bari, Italy, in 2010 and 2012, respectively, and his Ph.D. degree in environmental engineering, with a thesis on the synergistic use of synthetic aperture radar constellations for studying natural and anthropogenic phenomena, from the University of Basilicata, Potenza, Italy, in 2016. Over the years, he has held various positions, including as a NASA Postdoctoral Program fellow with the Jet Propulsion Laboratory (JPL), California Institute of Technology, Pasadena, CA, USA; a scientist in radar science and engineering with the JPL; and an associate project scientist in Earth system science with the University of California, Irvine, Irvine, CA, USA. Since 2021, he has been an assistant professor of civil and environmental engineering with the Department of Civil and Environmental Engineering, University of Houston (UH), Houston, TX, USA. He is also a guest scientist with the German Aerospace Center, Munich, Germany, and an adjunct professor of Earth and atmospheric science at the UH. He is a Member of IEEE.

Josef Mittermayer (josef.mittermayer@dlr.de) received his diploma degree in electrical engineering from the Technical University of Munich, Germany, in 1995, with a thesis on scanning synthetic aperture radar (SAR) processing; his M.S. degree in space system engineering from the Delft University of Technology, Delft, The Netherlands, in 2004; and his Ph.D. degree from the University of Siegen, Germany, in 2000, in the field of spotlight SAR processing. From 1994 to 2001, he was with the Signal Processing Group, Microwaves and Radar Institute, German Aerospace Center (DLR), Wessling, Germany. From 2002 to 2008, he worked on the *TerraSAR-X* project with the DLR. From January 2004 until the end of the commissioning phase, in 2008, he was the group leader and project manager of system engineering and calibration, one of the three subprojects that form the *TerraSAR-X* ground segment. In addition, he was technically responsible for the *TerraSAR-X* commissioning phase. He is currently a scientist with the Microwaves and Radar Institute, working in the field of SAR system engineering and SAR processing.

Matteo Nannini (matteo.nannini@dlr.de) received his laurea degree in telecommunication engineering from the University of Florence (2003), where his thesis was completed in collaboration with the Microwaves and Radar Institute, German Aerospace Center (DLR). He later received his Ph.D. degree in electrical engineering from the Karlsruhe Institute of Technology, with research focused on synthetic aperture radar (SAR) tomography. Since 2004, he has been with the Microwaves and Radar Institute, DLR, Germany, working on a range of topics, including SAR processing, SAR interferometry, SAR tomography, spectral estimation techniques, radar ice sounding, and persistent scatterer interferometry time-series analysis.

Konstantinos Papathanassiou (kostas.papathanassiou@dlr.de) received his Dipl.-Ing degree in 1994 and his Ph.D. degree in 1999 from the Technical University of Graz, Austria. From 1992 to 1994, he was with the Institute for Digital Image Processing, Joanneum Research, Graz. Between 1995 and 1999, he worked at the Microwaves and

Radar Institute, German Aerospace Center, Oberpfaffenhofen, Germany. From 1999 to 2000, he was a European Union postdoctoral fellow with Applied Electromagnetics, St. Andrews, U.K. In October 2000, he returned to the Microwaves and Radar Institute, where he is a senior scientist leading the information retrieval research group. He is a Fellow of IEEE.

Matteo Pardini (matteo.pardini@dlr.de) received his M.Eng. degree (cum laude) in telecommunication engineering and his Ph.D. degree in information engineering from the University of Pisa, Pisa, Italy, in 2006 and 2010, respectively. In January 2010, he joined the Department of Radar Concepts, Microwaves and Radar Institute, German Aerospace Center, Oberpfaffenhofen, Germany, as a research scientist, after a visiting research period from August to December 2009. In 2017, he was a visiting scientist with the Department of Geographical Sciences, University of Maryland, College Park, College Park, MD, USA.

Muriel Pinheiro (muriel.pinheiro@esa.int) received her B.S. degree in electronic engineering and her M.S. degree in telecommunications from the Aeronautical Technological Institute, So Jos dos Campos, Brazil, in 2009 and 2010, respectively, and her Dr.-Ing. degree (with honors) from the Karlsruhe Institute of Technology, Karlsruhe, Germany, in 2016. From 2009 to 2010, she was with Bradar, working on the development of calibration algorithms for airborne synthetic aperture radar (SAR) interferometry. From 2011 to 2021, she was with the Microwaves and Radar Institute, German Aerospace Center, Wessling, Germany, where she was a member of the Multimodal Algorithms Group. Since 2021, she has been with the European Space Agency, Frascati, Italy, as a calibration and validation engineer for SAR missions, with a special focus on the quality assurance of *Sentinel-1* products.

Pau Prats-Iraola (pau.prats@dlr.de) was born in Madrid, Spain, in 1977. He received his Ingeniero degree and his Ph.D. degree, both in telecommunications engineering, from the Universitat Politècnica de Catalunya (UPC), Barcelona, Spain, in 2001 and 2006, respectively. From 2002 to 2006, he was with the Department of Signal Theory and Communications, UPC, where he worked in the field of airborne repeat-pass interferometry and airborne differential synthetic aperture radar (SAR) interferometry. In 2006, he joined the Microwaves and Radar Institute, German Aerospace Center, Wessling, Germany, where, since 2009, he has been the head of the Multimodal Algorithms Group. He is the responsible and main developer of the TanDEM-X interferometric processor, an end-to-end processing chain for data acquired by the *TerraSAR-X* and *TanDEM-X* satellites, which has been used to demonstrate novel SAR acquisition modes and techniques. He is a Fellow of IEEE.

Paola Rizzoli (paola.rizzoli@dlr.de) received her B.Sc. (2003) and M.Sc. (2006) degrees in telecommunication engineering from Politecnico di Milano, Milan, Italy, and her Ph.D. degree (2018, summa cum laude) in electrical engineering and information technology from the Karlsruhe Institute of Technology, Karlsruhe, Germany. From 2006 to 2008, she was with Politecnico di Milano and Aresys. At the end of 2008, she joined the Microwaves and Radar Institute, German Aerospace Center, Oberpfaffenhofen, Germany, TanDEM-X missions for the generation of the global TanDEM-X digital elevation model (DEM). Since 2016, she has led the Radar Science Group, Department of Satellite SAR Systems, being responsible for the final performance assessment of the global TanDEM-X DEM and the generation of the global TanDEM-X forest/nonforest map. Her research interests include synthetic aperture radar systems design, data reduction techniques, estimation theory, signal processing, and artificial intelligence. She is a Member of IEEE.

Marc Rodriguez-Cassola (marc.rodriguez@dlr.de) received his Ingeniero degree in telecommunication engineering from Universidad Publica de Navarra, Pamplona, Spain, in 2000 and his Dr.-Ing. degree in electrical engineering from the Karlsruhe Institute of Technology, Karlsruhe, Germany, in 2012. From 2000 to 2001, he was a radar hardware engineer with CETP/CNRS, Saint Maur des Fosses, France. From 2001 to 2003, he was a software engineer with Altran Consulting, Germany. Since 2003, he has been with the Microwaves and Radar Institute, German Aerospace Center, Wessling, Germany, where he works on airborne and spaceborne synthetic aperture radar system analysis and data processing.

Achim Roth (achim.roth@dlr.de) received his Dipl.-Ing. degree in geodesy from the University of Karlsruhe, Karlsruhe, Germany, in 1987. In 1987, he joined the German Aerospace Center (DLR) for the development and implementation of an operational synthetic aperture radar (SAR) geocoding system for the European Remote Sensing and X-SAR missions. Since 1991, he has led the SAR Topography team at the German Remote Sensing Data Center, DLR, Germany. From 2000 to 2004, he was the Shuttle Radar Topography Mission (SRTM)/X-SAR ground segment manager. Since 2002, he has been the *TerraSAR-X* science coordinator. He has contributed to the SRTM and is currently involved in the TerraSAR-X and TanDEM-X missions.

Maximilian Schandri (maximilian.schandri@dlr.de) received his B.Sc. and M.Sc. degrees in physics from Friedrich-Alexander-Universität Erlangen-Nürnberg, Germany, in 2018. In 2018, he joined the Microwaves and Radar Institute, German Aerospace Center, Wessling, Germany. There, he started as a research scientist, performing analysis for future synthetic aperture radar (SAR) satellite missions. He is currently involved in the acquisition planning for the TanDEM-X mission. For the geostationary mission proposal HydroTerra, he contributed to the SAR performance analysis.

Rolf Scheiber (rolf.scheiber@dlr.de) received his Dipl.-Ing. (M.Sc.) degree in electrical engineering from the Technical University of Munich, Germany, in 1994 and his Dr.-Ing. (Ph.D.) degree in 2003 from the University of Karlsruhe, Germany. Since 1994, he has been with the

Microwaves and Radar Institute, German Aerospace Center (DLR), Germany, where he developed the first operational high-precision interferometric synthetic aperture radar (SAR) processor for the Experimental SAR airborne sensor. Since 2001, he has headed the Signal Processing Group within the Department of SAR Technology, where he supervises the DLR's airborne SAR processing activities, including the new Digital Beamforming airborne SAR system.

Ulrich Steinbrecher (ulrich.steinbrecher@dlr.de) received his Dipl.-Ing. degree in electrical engineering/communication from the University of Siegen, Siegen, Germany, in 1990. In 1990, he started his career with the German Aerospace Center, Wessling, Germany, with the development of a synthetic aperture radar (SAR) raw data simulator. Then, he was in software development with the X-SAR processor and with the U.S.–Italian–German Spaceborne Imaging Radar-C/X-SAR missions in 1994. When the data were in-house, he concentrated on aspects of the operational SAR processing of high data volumes. In 1995, he pioneered a completely automatic SAR processing system based on a robot-maintained mass memory archive. Before he became responsible for the development of the raw data analysis and screening system for the Shuttle Radar Topography Mission (SRTM), he developed the software for a phase-preserving scanning SAR processor for *Radarsat-1*. In the time between the SRTM and the start of the *TerraSAR-X* project, he left the SAR domain for two years and contributed to the Scanning Imaging Absorption Spectrometer for Atmospheric Chartography limb processing system. Since 2002, he has been concerned with the *TerraSAR-X* radar system, and with the launch of the satellite, in 2007, he was responsible for *TerraSAR-X* instrument operations.

Barbara Schweisshelm (barbara.schweisshelm@dlr.de) is with the Remote Sensing Technology Institute, German Aerospace Center, Germany.

Michelangelo Villano (michelangelo.villano@dlr.de) received his B.Sc. and M.Sc. degrees (with honors) in telecommunication engineering from the Sapienza University of Rome, Rome, Italy, in 2006 and 2008, respectively, and his Ph.D. degree (with honors) in electrical engineering and information technology from the Karlsruhe Institute of Technology, Karlsruhe, Germany, in 2016. From 2008 to 2009, he was a young graduate trainee with the European Space Research and Technology Center, European Space Agency, Noordwijk, The Netherlands. Since 2009, he has been with the Microwaves and Radar Institute, German Aerospace Center, Wessling, Germany, where he is currently the head of the NewSpace SAR Research Group. In 2017, he was a visiting research scientist with the Communications, Tracking, and Radar Division, NASA Jet Propulsion Laboratory, Pasadena, CA, USA. Since 2019, he has also been a lecturer with Ulm University, Ulm, Germany. He is a Senior Member of IEEE.

Leena Julia Warmedinger (leenajulia.warmedinger@dlr.de) received her B.Sc. and M.Sc. degrees in environmental engineering from the Technical University of Munich in 2017 and 2020, respectively. In 2020, she joined the German Remote Sensing Data Center, German Aerospace Center, Wessling, Germany, where she is involved in the editing of the TanDEM-X digital elevation model for hydrographic applications.

Birgit Wessel (birgit.wessel@dlr.de) received her diploma degree in geodesy from the University of Hanover, Hanover, Germany, in 2000 and her Ph.D. degree (Dr.-Ing. degree) in geodesy/remote sensing from the Technical University of Munich (TUM), Munich, Germany, in 2006. From 2000 to 2005, she was with the Institute for Photogrammetry and Cartography, TUM. In 2005, she joined the German Remote Sensing Data Center, German Aerospace Center, Germany. Currently, she leads digital elevation model (DEM) calibration and mosaicking developments for the TerraSAR-X Add-On for Digital Elevation Measurement mission and is responsible for the PolarDEM product suite. Her research focuses on synthetic aperture radar image and DEM applications and DEM adjustment and validation.

Gerhard Krieger (gerhard.krieger@dlr.de) received his Dipl.-Ing. (M.S.) and Dr.-Ing. (Ph.D., with honors) degrees in electrical and communication engineering from the Technical University of Munich, Germany, in 1992 and 1999, respectively. From 1992 to 1999, he was with Ludwig Maximilians University, Munich, where he conducted multidisciplinary research on neuronal modeling and nonlinear information processing in biological and technical vision systems. Since 1999, he has been with the Microwaves and Radar Institute, German Aerospace Center, Oberpfaffenhofen, Germany, where he started as a research associate, developing signal processing algorithms for a novel forward-looking radar system employing digital beamforming on receive. From 2001 to 2007, he led the New SAR Missions Group, which pioneered the development of advanced bistatic and multistatic radar systems, such as *TanDEM-X for Digital Elevation Measurement*, as well as innovative multichannel synthetic aperture radar (SAR) techniques and algorithms for high-resolution wide swath SAR imaging. Since 2008, he has been the head of the Department of Radar Concepts, which hosts about 40 scientists focusing on new SAR techniques, missions, and applications. He is a Fellow of IEEE.

Manfred Zink (manfred.zink@dlr.de) received his Dipl.-Ing. degree in physics from the Technical University of Graz, Graz, Austria, in 1987, and the Dr.-Ing. degree in aerospace engineering and geodesy from the University of Stuttgart, Stuttgart, Germany, in 1993. In 1988, he joined the Microwave and Radar Institute, German Aerospace Center (DLR). He has pioneered calibration techniques for both air-and spaceborne SAR sensors and was responsible for building up the Oberpfaffenhofen calibration site. From 2000 to 2005, he was with the European Space Agency (ESA) and was responsible for the calibration/validation of the ASAR onboard ENVISAT. In 2005, he returned to the Microwaves and Radar Institute at DLR, where he is currently heading

the Satellite SAR Systems Department. From 2006 to 2015 he was leading the TanDEM-X ground segment project. He was the General Chairman of the European SAR Conference (EUSAR) in 2014 and 2024.

Alberto Moreira (alberto.moreira@dlr.de) is the director of the Microwaves and Radar Institute, German Aerospace Center, Germany, and a full professor with the Karlsruhe Institute of Technology, Karlsruhe, Germany, in the field of microwave remote sensing. He has been contributing to the advancement of synthetic aperture radar (SAR) systems with innovative concepts, technologies, and associated signal processing for more than 35 years. The TanDEM-X mission, led by the Microwaves and Radar Institute, is the first bistatic spaceborne SAR system consisting of two satellites flying in close formation and has generated a global high-resolution digital elevation model of Earth with unprecedented accuracy. Prof. Moreira is the initiator and principal investigator of this mission. He served as president of the IEEE Geoscience and Remote Sensing Society (GRSS) in 2010 and is the recipient of several international awards, including the IEEE Kiyo Tomiyasu Technical Field Award (2007), the GRSS Distinguished Achievement Award (2014), and the IEEE Dennis J. Picard Medal for Radar Technologies and Applications (2023). He is a Fellow of IEEE.

REFERENCES

[1] "Joint CSA, INTA & DLR Call: RADARSAT constellation - PAZ - TerraSAR-X - TanDEM-X – Missions." TanDEM-X Science Server. Accessed: 2024. [Online]. Available: https://tandemx-science.dlr.de

[2] "The TanDEM-X 30m edited digital elevation model (EDEM) and DEM change maps (DCM)." EOC Geoservice. Accessed: 2023. [Online]. Available: https://geoservice.dlr.de/web/dataguide/tdm30/

[3] M. Zink et al., "TanDEM-X: 10 years of formation flying bistatic SAR interferometry," *IEEE J. Sel. Topics Appl. Earth Observ. Remote Sens.*, vol. 14, pp. 3546–3565, 2021, doi: 10.1109/JSTARS.2021.3062286.

[4] G. Krieger et al., "TanDEM-X: A radar interferometer with two formation flying satellites," *Acta Astronaut.*, vol. 89, pp. 83–98, Aug./Sep. 2013, doi: 10.1016/j.actaastro.2013.03.008.

[5] G. Krieger et al., "TanDEM-X: A satellite formation for high-resolution SAR interferometry," *IEEE Trans. Geosci. Remote Sens.*, vol. 45, no. 11, pp. 3317–3341, Nov. 2007, doi: 10.1109/TGRS.2007.900693.

[6] M. Zink et al., "TanDEM-X: The new global DEM takes shape," *IEEE Geosci. Remote Sens. Mag.*, vol. 2, no. 2, pp. 8–23, Jul. 2014, doi: 10.1109/MGRS.2014.2318895.

[7] R. Werninghaus and S. Buckreuss, "The TerraSAR-X mission and system design," *IEEE Trans. Geosci. Remote Sens.*, vol. 48, no. 2, pp. 606–614, Feb. 2010, doi: 10.1109/TGRS.2009.2031062.

[8] W. Pitz and D. Miller, "The TerraSAR-X satellite," *IEEE Trans. Geosci. Remote Sens.*, vol. 48, no. 2, pp. 615–622, Feb. 2010, doi: 10.1109/TGRS.2009.2037432.

[9] R. Kahle, B. Schlepp, F. Meissner, M. Kirschner, and R. Kiehling, "The TerraSAR-X/TanDEM-X formation acquisition – From planning to realization," *J. Astronautical Sci.*, vol. 59, no. 3, pp. 564–584, 2012, doi: 10.1007/s40295-014-0003-3.

[10] A. Moreira et al., "TanDEM-X: A TerraSAR-X add-on satellite for single-pass SAR interferometry," in *Proc. Int. Geosci. Remote Sens. Symp. (IGARSS)*, Anchorage, AK USA, 2004, vol. 2, pp. 1000–1003, doi: 10.1109/IGARSS.2004.1368578.

[11] A. Bojarski et al., "TanDEM-X long-term system performance after 10 years of operation," *IEEE J. Sel. Topics Appl. Earth Observ. Remote Sens.*, vol. 14, pp. 2522–2534, 2021, doi: 10.1109/JSTARS.2021.3055546.

[12] P. Rizzoli et al., "Generation and performance assessment of the global TanDEM-X digital elevation model," *ISPRS J. Photogramm. Remote Sens.*, vol. 132, pp. 119–139, Oct. 2017, doi: 10.1016/j.isprsjprs.2017.08.008.

[13] M. Bachmann et al., "The TanDEM-X mission phases—Ten years of bistatic acquisition and formation planning," *IEEE J. Sel. Topics Appl. Earth Observ. Remote Sens.*, vol. 14, pp. 3504–3518, 2021, doi: 10.1109/JSTARS.2021.3065446.

[14] M. Lachaise, T. Fritz, and R. Bamler, "The dual-baseline phase unwrapping correction framework for the TanDEM-X mission part 1: Theoretical description and algorithms," *IEEE Trans. Geosci. Remote Sens.*, vol. 56, no. 2, pp. 780–798, Feb. 2018, doi: 10.1109/TGRS.2017.2754923.

[15] M. Bachmann, B. Bräutigam, D. Schulze, G. Krieger, and M. Zink, "TanDEM-X acquisition plan and DEM performance in the third year of operation," in *Proc. Asia-Pacific Conf. Synthetic Aperture Radar (APSAR)*, Tsukuba, Japan, 2013, pp. 12–15.

[16] M. Martone, B. Bräutigam, P. Rizzoli, N. Yague-Martinez, and G. Krieger, "Enhancing interferometric SAR performance over sandy areas: Experience from the TanDEM-X mission," *IEEE J. Sel. Topics Appl. Earth Observ. Remote Sens.*, vol. 9, no. 3, pp. 1036–1046, Mar. 2016, doi: 10.1109/JSTARS.2015.2418537.

[17] J.-L. Bueso-Bello et al., "Performance analysis of TanDEM-X quad-polarization products in pursuit monostatic mode," *IEEE J. Sel. Topics Appl. Earth Observ. Remote Sens.*, vol. 10, no. 5, pp. 1853–1869, May 2017, doi: 10.1109/JSTARS.2017.2663323.

[18] J. Bueso-Bello, P. Prats-Iraola, M. Martone, J. Reimann, U. Steinbrecher, and P. Rizzoli, "Performance evaluation of TanDEM-X quad-polarization products in bistatic mode," *IEEE J. Sel. Topics Appl. Earth Observ. Remote Sens.*, vol. 11, no. 3, pp. 787–799, Mar. 2018, doi: 10.1109/JSTARS.2018.2790944.

[19] B. Wessel et al., "Concept and first example of TanDEM-X high-resolution DEM," in *Proc. 11th Eur. Conf. Synthetic Aperture Radar (EUSAR)*, Hamburg, Germany, 2016, pp. 1–4.

[20] M. Lachaise and B. Schweißhelm, "The TanDEM-X 30m DEM change maps: Applications and further developments," in *Proc. 15th Eur. Conf. Synthetic Aperture Radar*, Munich, Germany, 2024, pp. 901–906.

[21] M. Lachaise et al., "The TanDEM-X 30m edited DEM & DEM change maps: The new products in 30m posting," in *Proc. TerraSAR-X/TanDEM-X Sci. Team Meeting*, 2023.

[22] M. Bachmann et al., "TerraSAR-X and TanDEM-X after 13 years of joint SAR and DEM mission," in *Proc. IEEE Int. Geosci. Remote Sens. Symp. (IGARSS)*, Pasadena, CA, USA, 2023, pp. 1325–1328, doi: 10.1109/IGARSS52108.2023.10281959.

[23] A. Alonso-González et al., "Joint PAZ & TanDEM-X mission interferometric experiments: Interoperability and products," *IEEE J. Sel. Topics Appl. Earth Observ. Remote Sens.*, vol. 14, pp. 6069–6082, 2021, doi: 10.1109/JSTARS.2021.3084401.

[24] B. Wessel, M. Huber, C. Wohlfart, U. Marschalk, D. Kosmann, and A. Roth, "Accuracy assessment of the global TanDEM-X digital elevation model with GPS data," *ISPRS J. Photogramm. Remote Sens.*, vol. 139, pp. 171–182, May 2018, doi: 10.1016/j.isprsjprs.2018.02.017.

[25] J. Mittermayer et al., "MirrorSAR: An HRWS add-on for single-pass multi-baseline SAR interferometry," *IEEE Trans. Geosci. Remote Sens.*, vol. 60, pp. 1–18, 2021, doi: 10.1109/TGRS.2021.3132384.

[26] B. Wessel et al., "TanDEM-X PolarDEM 90 m of Antarctica: Generation and error characterization," *Cryosphere*, vol. 15, no. 11, pp. 5241–5260, 2021, doi: 10.5194/tc-15-5241-2021.

[27] J.-L. Bueso-Bello et al., "The global water body layer from TanDEM-X interferometric SAR data," *Remote Sens.*, vol. 13, no. 24, Dec 2021, Art. no. 5069, doi: 10.3390/rs13245069.

[28] C. Gonzalez, M. Bachmann, J.-L. Bueso-Bello, P. Rizzoli, and M. Zink, "A fully automatic algorithm for editing the TanDEM-X global DEM," *Remote Sens.*, vol. 12, no. 23, Dec. 2020, Art. no. 3961, doi: 10.3390/rs12233961.

[29] "DLR Geoservice web." EOC Geoservice. Accessed: 2023. [Online]. Available: https://geoservice.dlr.de/web/

[30] S. Abdullahi, B. Wessel, M. Huber, A. Wendleder, A. Roth, and C. Künzer, "Estimating penetration-related X-band InSAR elevation bias: A study over the Greenland ice sheet," *Remote Sens.*, vol. 11, no. 24, Dec 2021, Art. no. 2903, doi: 10.3390/rs11242903.

[31] D. Abdullahi, B. Burgess, B. Wessel, L. Copeland, and A. Roth, "Quantifying the impact of X-band InSAR penetration bias on elevation change and mass balance estimation," *Ann. Glaciol.*, vol. 64, no. 92, 2024, doi: 10.1017/aog.2024.7.

[32] "TanDEM-X PolarDEM" Deutsches Zentrum für Luft- und Raumfahrt (DLR)." Accessed: May 15, 2024. [Online]. Available: https://www.dlr.de/en/eoc/research-transfer/projects-missions/tandem-x-polardem

[33] M. Lachaise and T. Fritz, "Update of the interferometric processing algorithms for the Tan-DEM-X high resolution DEMs," in *Proc. 11th Eur. Conf. Synthetic Aperture Radar (EUSAR)*, Hamburg, Germany, 2016, pp. 1–4.

[34] M. Lachaise, B. Schweisshelm, and T. Fritz, "The new TanDEM-X change DEM: Specifications and interferometric processing," in *Proc. IEEE Latin Amer. GRSS ISPRS Remote Sens. Conf. (LAGIRS)*, 2020, pp. 646–651, doi: 10.1109/LAGIRS48042.2020.9165638.

[35] B. Wessel, "TanDEM-X ground segment – DEM products specification document," EOC, DLR, Oberpfaffenhofen, Germany, Public Document TD-GS-PS-0021, 2018. [Online] Available: https://tandemx-science.dlr.de/pdfs/TD-GS-PS-0021_DEM-Product-Specification_v3.1.pdf

[36] M. Lachaise et al., "TanDEM-X 30m DEM change maps product description," 2023. [Online]. Available: https://geoservice.dlr.de/web/dataguide/tdm30/pdfs/TD-GS-PS-0216_TanDEM-X_30m_DEM_Change_Maps_Product_Description_1.0.pdf

[37] T. Esch et al., "World settlement footprint 3D - A first three-dimensional survey of the global building stock," *Remote Sens. Environ.*, vol. 270, Mar. 2022, Art. no. 112877, doi: 10.1016/j.rse.2021.112877.

[38] M. Marconcini, A. Metz-Marconcini, T. Esch, and N. Gorelick, 2021. "Understanding current trends in global urbanisation – The world settlement footprint suite," in *Proc. 12th Int. Symp. Digit. Earth GI Forum*, Salzburg, Austria, 2021.

[39] P. Lopez-Dekker, B. Chapron, and H. Johnsen, "Observations of sea surface winds and sea surface deformation with the harmony mission," in *Proc. 13th Eur. Conf. Synthetic Aperture Radar (EUSAR)*, 2021, pp. 1–4.

[40] M. Martone, P. Rizzoli, and G. Krieger, "Volume decorrelation effects in TanDEM-X interferometric SAR data," *IEEE Geosci. Remote Sens. Lett.*, vol. 13, no. 12, pp. 1812–1816, Dec. 2016, doi: 10.1109/LGRS.2016.2614103.

[41] P. Rizzoli, L. Dell'Amore, J.-L. Bueso-Bello, N. Gollin, D. Carcereri, and M. Martone, "On the derivation of volume decorrelation from TanDEM-X bistatic coherence," *IEEE J. Sel. Topics Appl. Earth Observ. Remote Sens.*, vol. 15, pp. 3504–3518, 2022, doi: 10.1109/JSTARS.2022.3170076.

[42] M. Martone et al., "The global forest/non-forest map from TanDEM-X interferometric SAR data," *Remote Sens. Environ.*, vol. 205, pp. 352–373, Feb. 2018, doi: 10.1016/j.rse.2017.12.002.

[43] J.-L. Bueso-Bello, D. Carcereri, M. Martone, C. González, P. Posovszky, and P. Rizzoli, "Deep learning for mapping tropical forests with TanDEM-X bistatic InSAR data," *Remote Sens.*, vol. 14, no. 16, 2022, Art. no. 3981, doi: 10.3390/rs14163981.

[44] M. J. Soja, H. Persson, and L. M. H. Ulander, "Estimation of forest height and canopy density from a single InSAR correlation coefficient," *IEEE Geosci. Remote Sens. Lett.*, vol. 12, no. 3, pp. 646–650, Mar. 2015, doi: 10.1109/LGRS.2014.2354551.

[45] F. Kugler, D. Schulze, I. Hajnsek, H. Pretzsch, and K. Papathanassiou, "TanDEM-X Pol-InSAR performance for forest height estimation," *IEEE Trans. Geosci. Remote Sens.*, vol. 52, no. 10, pp. 6404–6422, Oct. 2014, doi: 10.1109/TGRS.2013.2296533.

[46] H. J. Persson and J. E. S. Fransson, "Comparison between TanDEM-X and ALS based estimation of above ground biomass and tree height in boreal forests," *Scand. J. For. Res.*, vol. 32, no. 4, pp. 306–319, 2017, doi: 10.1080/02827581.2016.1220618.

[47] R. Treuhaft et al., "Tropical-forest biomass estimation at X-Band from the spaceborne TanDEM-X interferometer," *IEEE Geosci. Remote Sens. Lett.*, vol. 12, no. 2, pp. 239–243, Feb. 2015, doi: 10.1109/LGRS.2014.2334140.

[48] S. Solberg, E. Næsset, T. Gobakken, and O. M. Bollandsås, "Forest biomass change estimated from height change in interferometric SAR height models," *Carbon Balance Manage.*, vol. 9, no. 1, pp. 1–12, 2014, doi: 10.1186/s13021-014-0005-2.

[49] H. J. Persson, H. Olsson, M. J. Soja, L. M. Ulander, and J. E. Fransson, "Experiences from large-scale forest mapping of Sweden using TanDEM-X data," *Remote Sens.*, vol. 9, no. 12, 2017, Art. no. 1253, doi: 10.3390/rs9121253.

[50] H. J. Persson, M. J. Soja, J. E. S. Fransson, and L. M. H. Ulander, "National forest biomass mapping using the two-level model,"

IEEE J. Sel. Topics Appl. Earth Observ. Remote Sens., vol. 13, pp. 6391–6400, 2020, doi: 10.1109/JSTARS.2020.3030591.

[51] M. J. Soja, H. J. Persson, and L. M. H. Ulander, "Modeling and detection of deforestation and forest growth in multitemporal TanDEM-X data," *IEEE J. Sel. Topics Appl. Earth Observ. Remote Sens.*, vol. 11, no. 10, pp. 3548–3563, Oct. 2018, doi: 10.1109/JSTARS.2018.2851030.

[52] J. I. H. Askne, J. E. S. Fransson, M. Santoro, M. J. Soja, and L. M. H. Ulander, "Model-based biomass estimation of a hemi-boreal forest from multitemporal TanDEM-X acquisitions," *Remote Sens.*, vol. 5, no. 11, pp. 5574–5597, 2013, doi: 10.3390/rs5115574.

[53] M. Schlund, F. von Poncet, S. Kuntz, C. Schmullius, D. H. Hoekman, "TanDEM-X data for aboveground biomass retrieval in a tropical peat swamp forest," *Remote Sens. Environ.*, vol. 158, pp. 255–266, Mar. 2015, doi: 10.1016/j.rse.2014.11.016.

[54] R. Guliaev, V. Cazcarra-Bes, M. Pardini, and K. Papathanassiou, "Forest height estimation by means of TanDEM-X InSAR and waveform lidar data," *IEEE J. Sel. Topics Appl. Earth Observ. Remote Sens.*, vol. 14, pp. 3084–3094, 2021, doi: 10.1109/JSTARS.2021.3058837.

[55] C. Choi et al., "Large-scale forest height mapping by combining TanDEM-X and GEDI data," *IEEE J. Sel. Topics Appl. Earth Observ. Remote Sens.*, vol. 16, pp. 2374–2385, 2023, doi: 10.1109/JSTARS.2023.3244866.

[56] W. Qi and R. O. Dubayah, "Combining Tandem-X InSAR and simulated GEDI lidar observations for forest structure mapping," *Remote Sens. Environ.*, vol. 187, pp. 253–266, Dec. 2016, doi: 10.1016/j.rse.2016.10.018.

[57] W. Qi et al., "Improved forest height estimation by fusion of simulated GEDI Lidar data and TanDEM-X InSAR data," *Remote Sens. Environ.*, vol. 221, pp. 621–634, Feb. 2019, doi: 10.1016/j.rse.2018.11.035.

[58] H. Chen, S. R. Cloude, and J. C. White, "Using GEDI waveforms for improved TanDEM-X forest height mapping: A combined SINC + Legendre approach," *Remote Sens.*, vol. 13, no. 15, 2021, Art. no. 2882, doi: 10.3390/rs13152882.

[59] M. Schlund, A. Wenzel, N. Camarretta, C. Stiegler, and S. Erasmi, "Vegetation canopy height estimation in dynamic tropical landscapes with TanDEM-X supported by GEDI data," *Methods Ecol. Evol.*, vol. 14, no. 7, pp. 1639–1656,2022, doi: 10.1111/2041-210X.13933.

[60] A. Alonso-González, H. Joerg, K. Papathanassiou, and I. Hajnsek, "Dual-polarimetric agricultural change analysis of long baseline TanDEM-X time series data," in *Proc. IEEE Int. Geosci. Remote Sens. Symp. (IGARSS)*, Beijing, China, 2016, pp. 325–328, , doi: 10.1109/IGARSS.2016.7729077.

[61] A. Alonso-Gonzalez and K. P. Papathanassiou, "Multi-frequency polarimetric change analysis for agricultural monitoring," in *Proc. 14th Eur. Conf. Synthetic Aperture Radar*, Leipzig, Germany, 2022, pp. 1–6.

[62] Milillo et al., "Heterogeneous retreat and ice melt of Thwaites Glacier, West Antarctica," *Sci. Adv.*, vol. 5, no. 1, 2019, Art. no. eaau3433, doi: 10.1126/sciadv.aau3433.

[63] S. Leinss and P. Bernhard, "TanDEM-X: Deriving InSAR height changes and velocity dynamics of great Aletsch Glacier," *IEEE J. Sel. Topics Appl. Earth Observ. Remote Sens.*, vol. 14, pp. 4798–4815, 2021, doi: 10.1109/JSTARS.2021.3078084.

[64] P.-L. Vlieghe, "Revealing the recent height changes of the great Aletsch Glacier using TanDEM-X DEM series," Master thesis, ETH Zurich, Zurich Switzerland, 2023.

[65] E. Berthier et al., "Measuring glacier mass changes from space - A review," *Rep. Prog. Phys.*, vol. 86, no. 3, pp. 1–32, 2023, doi: 10.1088/1361-6633/acaf8e.

[66] W. Abdel Jaber, H. Rott, D. Floricioiu, J. Wuite, and N. Miranda, "Heterogeneous spatial and temporal pattern of surface elevation change and mass balance of the Patagonian ice fields between 2000 and 2016," *Cryosphere*, vol. 13, no. 9, pp. 2511–2535, 2019, doi: 10.5194/tc-13-2511-2019.

[67] L. Andreas, M. A. Lange, S. F. Ackley, and P. Wadhams, "Roughness of Weddell Sea ice and estimates of the air-ice drag coefficient," *J. Geophys. Res.: Oceans*, vol. 98, no. C7, pp. 12,439–12,452, 1993, doi: 10.1029/93JC00654.

[68] W. Dierking, O. Lang, and T. Busche, "Sea ice local surface topography from single-pass satellite InSAR measurements: A feasibility study," *Cryosphere*, vol. 11, no. 4, pp. 1967–1985, 2017, doi: 10.5194/tc-11-1967-2017.

[69] S. Nghiem et al., "Remote sensing of Antarctic sea ice with coordinated aircraft and satellite data acquisitions," in *Proc. IEEE Int. Geosci. Remote Sens. Symp.*, Piscataway, NJ, USA: IEEE Press, 2018, pp. 8531–8534, doi: 10.1109/IGARSS.2018.8518550.

[70] L. Huang and I. Hajnsek, "A study of sea ice topography in the Weddell and Ross seas using dual-polarimetric TanDEM-X imagery," *Cryosphere*, vol. 18, no. 7, pp. 3117–3140, 2024, doi: 10.5194/tc-18-3117-2024.

[71] L. Huang, G. Fischer, and I. Hajnsek, "Antarctic snow-covered sea ice topography derivation from tanDEM-X using polarimetric SAR interferometry," *Cryosphere*, vol. 15, no. 12, pp. 5323–5344, 2021, doi: 10.5194/tc-15-5323-2021.

[72] P. Bernhard, S. Zwieback, S. Leins, and I. Hajnsek, "Mapping retrogressive thaw slumps using single-pass TanDEM-X observations," *IEEE J. Sel. Topics Appl. Earth Observ. Remote Sens.*, vol. 13, pp. 3263–3280, 2020, doi: 10.1109/JSTARS.2020.3000648.

[73] P. Bernhard, S. Zwieback, N. Bergner, and I. Hajnsek, "Assessing volumetric change distributions and scaling relations of retrogressive thaw slumps across the Arctic," *Cryosphere*, vol. 16, no. 1, pp. 1–15, 2022, doi: 10.5194/tc-16-1-2022.

[74] P. Bernhard, S. Zwieback, and I. Hajnsek, "Accelerated mobilization of organic carbon from retrogressive thaw slumps on the northern Taymyr Peninsula," *Cryosphere*, vol. 16, pp. 2819–2835, Jul. 2022, doi: 10.5194/tc-16-2819-2022.

[75] C. Gonzalez et al., "Need for mutual DEM calibration for monitoring of height changes from TanDEM-X DEM difference," in *Proc. Eur. Conf. Synthetic Aperture Radar (EUSAR)*, 2024.

[76] B. Lehner, K. Verdin, and A. Jarvis, and A. "New global hydrography derived from spaceborne elevation data," *Eos, Trans. Amer. Geophys. Union*, vol. 89, no. 10, pp. 93–94, 2008, doi: 10.1029/2008EO100001.

[77] B. Lehner, A. Roth, M. Huber, M. Anand, and M. Thieme, "A sharper look at the world's rivers and catchments," *Eos,*

Trans. Amer. Geophys. Union, vol. 103, pp. 1–10, Apr. 2022, doi: 10.1029/2022EO220167.

[78] L. Warmedinger et al., "The new hydrographic hydrosheds database derived from the tandem-X DEM," in *Proc. IEEE Int. Geosci. Remote Sens. Symp. (IGARSS)*, pp. 1485–1488, 2023, doi: 10.1109/IGARSS52108.2023.10282244.

[79] M. Huber et al., "Shaping the global high-resolution TanDEM-X digital elevation mode," *IEEE J. Sel. Topics Appl. Earth Observ. Remote Sens.*, vol. 14, pp. 7198–7212, 2021, doi: 10.1109/JSTARS.2021.3095178.

[80] P. Prats et al., "TAXI: A versatile processing chain for experimental TanDEM-X product evaluation," in *Proc. IEEE Int. Geosci. Remote Sens. Symp.*, 2010, pp. 4059–4062, doi: 10.1109/IGARSS.2010.5651002.

[81] M. Rodriguez-Cassola et al., "First bistatic spaceborne SAR experiments with TanDEM-X," *IEEE Geosci. Remote Sens. Lett.*, vol. 9, no. 1, pp. 33–37, Jan. 2012, doi: 10.1109/LGRS.2011.2158984.

[82] P. Lopez-Dekker, P. Prats, F. De Zan, D. Schulze, G. Krieger, and A. Moreira, "TanDEM-X first DEM acquisition: A crossing orbit experiment," *IEEE Geosci. Remote Sens. Lett.*, vol. 8, no. 5, pp. 943–947, Sep. 2011, doi: 10.1109/LGRS.2011.2127444.

[83] S. Wollstadt, P. Lòpez-Dekker, P. Prats-Iraola, F. De Zan, T. Busche, and G. Krieger, "1 and 5 day differential InSAR under crossing orbits with TerraSAR-X," in *Proc. IEEE Int. Geosci. Remote Sens. Symp.*, 2012, pp. 1868–1871, doi: 10.1109/IGARSS.2012.6350817.

[84] P. Prats et al., "Distributed imaging with TerraSAR-X and TanDEM-X," in *Proc. IEEE Int. Geosci. Remote Sens. Symp.*, Vancouver, BC, Canada, 2011, pp. 3963–3966, doi: 10.1109/IGARSS.2011.6050099.

[85] R. Scheiber, M. Keller, J. Fischer, C. Andreas, R. Horn, and I. Hajnsek, "Radar data processing, quality analysis and level-1b product generation for AGRISAR and EAGLE campaigns," in *Proc. AGRISAR EAGLE Campaigns Final Workshop*, Noordwijk, The Netherlands, 2007.

[86] T. Ainsworth, M. L. Preiss, N. Stacy, and J. S. Lee, "Quad-polarimetry and interferometry from repeat-pass dual-polarimetric SAR imagery," in *Proc. IEEE Int. Geosci. Remote Sens. Symp.*, pp. 2616–2619, 2007, doi: 10.1109/IGARSS.2007.4423381.

[87] N. Caldarella et al., "Retrieval of wind and total surface current vectors using experimental bidirectional along-track interferometric TanDEM-X data," *IEEE Trans. Geosci. Remote Sens.*, vol. 60, pp. 1–12, 2022, doi: 10.1109/TGRS.2022.3147490.

[88] G. Krieger, N. Gebert, and A. Moreira, "Unambiguous SAR signal reconstruction from nonuniform displaced phase center sampling," *IEEE Geosci. Remote Sens. Lett.*, vol. 1, no. 4, pp. 260–264, Oct. 2004, doi: 10.1109/LGRS.2004.832700.

[89] J.-H. Kim, M. Younis, P. Prats-Iraola, M. Gabele, and G. Krieger, "First spaceborne demonstration of digital beamforming for azimuth ambiguity suppression," *IEEE Trans. Geosci. Remote Sens.*, vol. 51, no. 1, pp. 579–590, Jan. 2013, doi: 10.1109/TGRS.2012.2201947.

[90] T. Kraus, G. Krieger, M. Bachmann, and A. Moreira, "Spaceborne demonstration of distributed SAR imaging with TerraSAR-X and TanDEM-X," *IEEE Geosci. Remote Sens. Lett.*, vol. 16, no. 11, pp. 1731–1735, Nov. 2019, doi: 10.1109/LGRS.2019.2907371.

[91] T. Kraus, B. Bräutigam, M. Bachmann, G. Krieger, and J. Mittermayer, "TerraSAR-X and TanDEM-X: A unique platform to demonstrate the capabilities of distributed SAR satellite systems," in *Proc. ONERA-DLR Aerosp. Symp. (ODAS)*, Oberpfaffenhofen, Germany, 2016.

[92] G. Krieger and A. Moreira, "Potential of digital beamforming in bi- and multistatic SAR," in *Proc. IEEE Int. Geosci. Remote Sens. Symp. (IGARSS) (IEEE Cat. No.03CH37477)*, 2003, vol. 1, pp. 527–529, doi: 10.1109/IGARSS.2003.1293831.

[93] G. Krieger and A. Moreira, "Spaceborne bi- and multistatic SAR: Potential and challenges," *IEE Proc. - Radar, Sonar Navigat.*, vol. 153, no. 3, pp. 184–198, 2006, doi: 10.1049/ip-rsn:20045111.

[94] M. Villano and G. Krieger, "Impact of azimuth ambiguities on interferometric performance," *IEEE Geosci. Rem. Sens. Lett.*, vol. 9, no. 5, pp. 896–900, Sep. 2012, doi: 10.1109/LGRS.2012.2187271.

[95] M. Villano and G. Krieger, "Accounting for azimuth ambiguities in interferometric performance analysis," in *Proc. IEEE Int. Geosci. Rem. Sens. Symp.*, 2012, pp. 299–302, doi: 10.1109/IGARSS.2012.6351578.

[96] D. Richter, M. Rodriguez-Cassola, M. Zonno, and P. Prats-Iraola, "Coherent azimuth ambiguity suppression based on linear optimum filtering of short along-track baseline SAR interferograms," in *Proc. 14th Eur. Conf. Synthetic Aperture Radar (EUSAR)*, Leipzig, Germany, 2022, pp. 1–5.

[97] M. Villano, M. N. Peixoto, N. Ustalli, J. Mittermayer, G. Krieger, and A. Moreira, "Decorrelating ambiguities in SAR interferometry through slight PRI variation," *IEEE Trans. Geosci. Remote Sens.*, vol. 60, pp. 1–13, 2022, doi: 10.1109/TGRS.2022.3227316.

[98] R. Scheiber, F. De Zan, P. Prats, L. Sant'Anna Araújo, M. Künemund, and L. Marotti, "Interferometric sea ice mapping with TanDEM-X: First experiments," in *Proc. IEEE Int. Geosci. Remote Sens. Symp.*, Vancouver, BC, Canada, 2011, pp. 3594–3597, doi: 10.1109/IGARSS.2011.6050001.

[99] M. Pinheiro, A. Reigber, and A. Moreira, "Large-baseline InSAR for precise topographic mapping: A framework for TanDEM-X large-baseline data," *Adv. Radio Sci.*, vol. 15, pp. 231–241, Sep. 2017, doi: 10.5194/ars-15-231-2017.

[100] M. Martone, B. Bräutigam, and G. Krieger, "Quantization effects in TanDEM-X data," *IEEE Trans. Geosci. Remote Sens.*, vol. 53, no. 2, pp. 583–597, Feb. 2015, doi: 10.1109/TGRS.2014.2325976.

[101] M. Martone, B. Bräutigam, and G. Krieger, "Azimuth-switched quantization for SAR systems and performance analysis on TanDEM-X data," *IEEE Geosci. Remote Sens. Lett.*, vol. 11, no. 1, pp. 181–185, Jan. 2014, doi: 10.1109/LGRS.2013.2251603.

[102] M. Martone, N. Gollin, P. Rizzoli, and G. Krieger, "Performance-optimized quantization for SAR and InSAR applications," *IEEE Trans. Geosci. Remote Sens.*, vol. 60, pp. 1–22, 2022, doi: 10.1109/TGRS.2022.3181237.

[103] N. Gollin, M. Martone, G. Krieger, and P. Rizzoli, "AI-based performance-optimized quantization for future SAR systems," in *Proc. IEEE Int. Geosci. Remote Sens. Symp. (IGARSS)*,

Pasadena, CA, USA, 2023, pp. 1771–1774, doi: 10.1109/IGARSS52108.2023.10282929.

[104] S. V. Baumgartner and G. Krieger, "Dual-platform large along-track baseline GMTI," *IEEE Trans. Geosci. Remote Sens.*, vol. 54, no. 3, pp. 1554–1574, Mar. 2016, doi: 10.1109/TGRS.2015.2483019.

[105] A. Reigber and A. Moreira, "First demonstration of airborne SAR tomography using multibaseline L-band data," *IEEE Trans. Geosci. Remote Sens.*, vol. 38, no. 5, pp. 2142–2152, Sep. 2000, doi: 10.1109/36.868873.

[106] S. Tebaldini, T. Nagler, H. Rott, and A. Heilig, "Imaging the internal structure of an alpine glacier via L-band airborne SAR tomography," *IEEE Trans. Geosci. Remote Sens.*, vol. 54, no. 12, pp. 7197–7209, Dec. 2016, doi: 10.1109/TGRS.2016.2597361.

[107] G. Krieger et al., "The tandem-L mission proposal: Monitoring earth's dynamics with high resolution SAR interferometry," in *Proc. IEEE Radar Conf.*, 2009, pp. 1–6, doi: 10.1109/RADAR.2009.4977077.

[108] M. Pardini, A. Torano-Caicoya, F. Kugler, and K. Papathanassiou, "Estimating and understanding vertical structure of forests from multibaseline TanDEM-X Pol-InSAR data," in *Proc. IEEE Int. Geosci. Remote Sens. Symp. (IGARSS)*, 2013, pp. 4344–4347, doi: 10.1109/IGARSS.2013.6723796.

[109] M. Nannini et al., "Coherence-based SAR tomography for spaceborne applications," *Remote Sens. Environ.*, vol. 225, pp. 107–114, May 2019, doi: 10.1016/j.rse.2019.01.040.

[110] F. Gini, F. Lombardini, and M. Montanari, "Layover solution in multibaseline SAR interferometry," *IEEE Trans. Aerosp. Electron. Syst.*, vol. 38, no. 4, pp. 1344–1356, Oct. 2002, doi: 10.1109/TAES.2002.1145755.

[111] J. Mittermayer, S. Wollstadt, P. Prats, P. López-Dekker, G. Krieger, and A. Moreira, "Bidirectional SAR imaging mode," *IEEE Trans. Geosci. Remote Sens.*, vol. 51, no. 1, pp. 601–614, Jan. 2013, doi: 10.1109/TGRS.2012.2202669.

GRS